This SI replaces the original version published on 16 Jun 2020. Figure captions and surrounding text for Figures S35-37 have been updated from 'G5-EG4-OH + MLB-EBOV GP Pseudotype' to 'G5-OH + VSV-EBOV-GP'.

ELECTRONIC SUPPORTING INFORMATION (ESI)

Probing scaffold size effects on multivalent lectin-glycan binding affinity, thermodynamics and antiviral properties using polyvalent glycan-gold nanoparticles

Rahman Basaran,[1] Darshita Budhadev,[1] Amy Kempf,[2] Inga Nehlmeier,[2] Nicole Hondow,[3] Stefan Pöhlmann,[2,4] Yuan Guo,[5] and Dejian Zhou[1,*]

[1] School of Chemistry and Astbury Centre for Structural Molecular Biology, University of Leeds, Leeds LS2 9JT, United Kingdom. Email: d.zhou@leeds.ac.uk.

[2] Infection Biology Unit, German Primate Center - Leibniz Institute for Primate Research, 37077 Göttingen, Germany.

[3] School of Chemical and Process Engineering, University of Leeds, Leeds LS2 9JT, United Kingdom.

[4] Faculty of Biology and Psychology, Georg-August-University Göttingen, 37073 Göttingen, Germany.

[5] School of Food Science and Nutrition, and Astbury Centre for Structural Molecular Biology, University of Leeds, Leeds LS2 9JT, United Kingdom.

Contents

1. Instrument and Methods

All moisture-sensitive reactions were performed in oven-dried glassware under a nitrogen atmosphere. Evaporations were carried out at reduced pressure using a Bruker rotary evaporator and a Virtis Benchtop K freeze dryer. Column chromatography was performed using silica gel 60 A, and the progress of the reactions was monitored by thin layer chromatography, TLC, analysis on aluminium sheets pre-coated with silica (Merck Silica Kieselgel 60 F_{254}), then for identifying the compounds present in the reaction mixture, TLC-plates were stained with iodine, orcinol, or *p*-anisaldehyde stains, commercially available. The polar lipoic acid-sugar derivatives were purified by size exclusion chromatography via Biogel P2 column using 20 mM ammonium formate as an eluent to yield the desired pure product.

All ^{1}H and ^{13}C NMR spectra were recorded on a Bruker AV4 NEO-500 (500 MHz for ^{1}H, 125 MHz for ^{13}C) and a Bruker AV3HD-400 (400 MHz for ^{1}H, 100 MHz for ^{13}C) spectrometer in appropriate undeuterated solvents. All chemical shifts (δs) are denoted in parts per million (ppm) calibrated using residual undeuterated solvents as internal references ($CDCl_3$: δ ^{1}H = 7.26 ppm, δ ^{13}C = 77.16 ppm; CD_3OD: δ ^{1}H = 3.31 ppm, δ ^{13}C = 49.15 ppm; D_2O: δ ^{1}H = 4.80 ppm). The coupling constants (*J*) are in parentheses and expressed in Hertz, Hz, and the peak patterns are indicated with the following abbreviations: s = singlet, d = doublet, t = triplet, q = quartet, m = multiplet, br = broad, dd = doublet of doublets, dt = doublet of triplets, td = triplet of doublets, dq= doublet of quartets, qt = quartet of triplets, ddd = doublet of doublet of doublets, dtd = doublet of triplet of doublets. High-resolution mass spectra (HR-MS) were obtained on a Bruker Daltonics MicroTOF mass spectrometer, and deconvoluted mass values (*m/z*) are reported in Daltons, and protein labelling efficiency was also calculated from the ratio of the integral of the labelled protein HR-MS peak to the sum of that of the labelled and unlabelled protein peaks. The mass spectrometry data were also collected using a Bruker HCT Ultra coupled to Ultimate 3000 HPLC (Thermo Scientific). Methanol was used as a solvent to ionise the products; this provides a high-precision detection of ionised samples by classifying the resulting ions by vacuum with respect to mass-charge ratios (*m/z*). UV-vis absorption spectra were recorded on either a Cary 60 UV-vis spectrophotometer (Agilent Technologies) over 200-800 nm using 1 mL quartz cuvette with an optical path length of 1 cm or on a Nanodrop 2000 spectrophotometer (Thermo Scientific) over the range of 200-800 nm using one drop of the solution with an optical path length of 1 mm.

2. GNP Synthesis and Characterisation

Gold nanoparticles with average diameters of ~13 and ~27 nm (abbreviated as G13 and G27, respectively) were synthesised in-house *via* our established protocols.[1-3] Details of the synthesis and purification procedures were given in the Experimental Section. The UV-vis, hydrodynamic diameter (D_h) histograms, and TEM images of the as-prepared G13 and G27 stocks were given in Figure S1 and Figure S2, respectively.

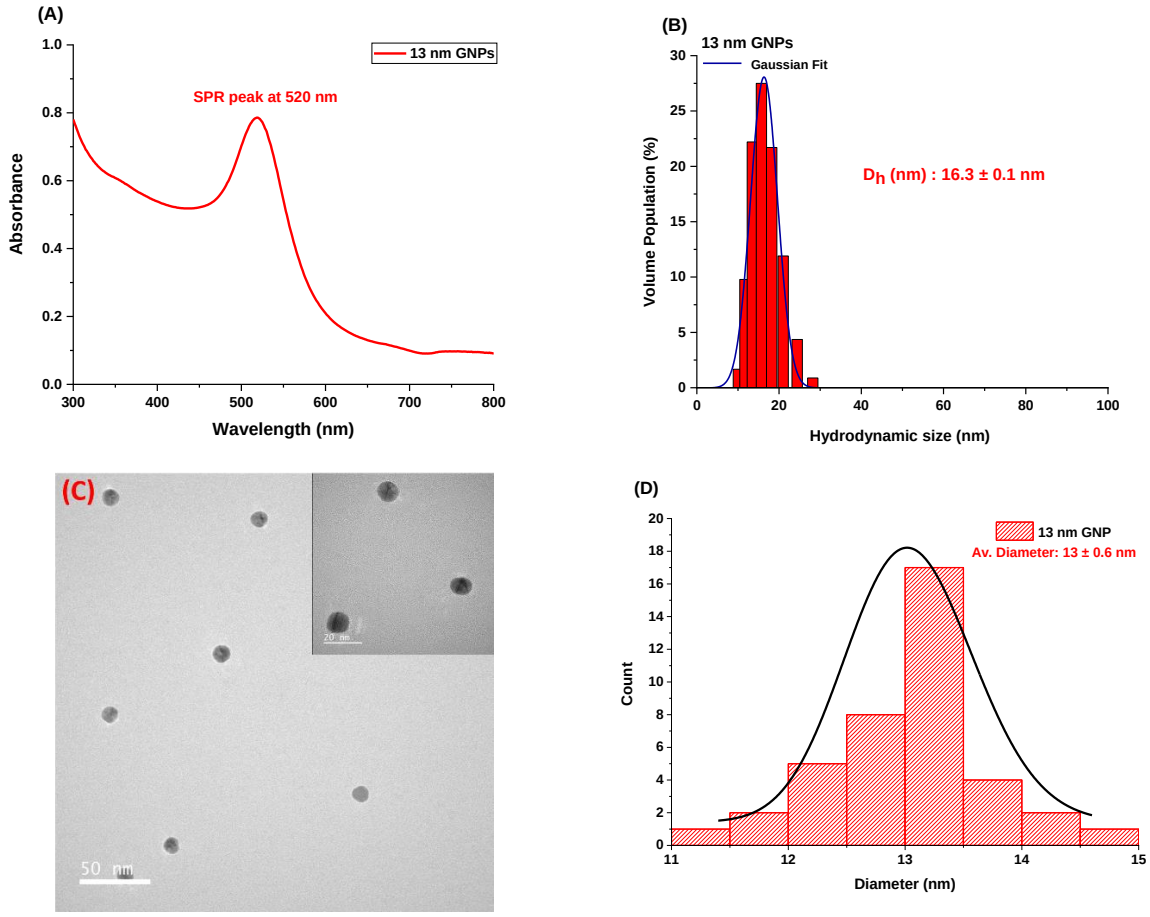

Figure S1. Characterisation of G13. (A) UV-vis absorption spectrum showing its SPR absorption peaking at ~520 nm, (B) D_h (volume population, fitted by Gaussian function) histogram showing a single Gaussian species with a D_h of ~16 nm; (C) A Typical TEM image (with higher magnification shown in the inset); (D) GNP diameter histogram measured by TEM fitted by Gaussian function.

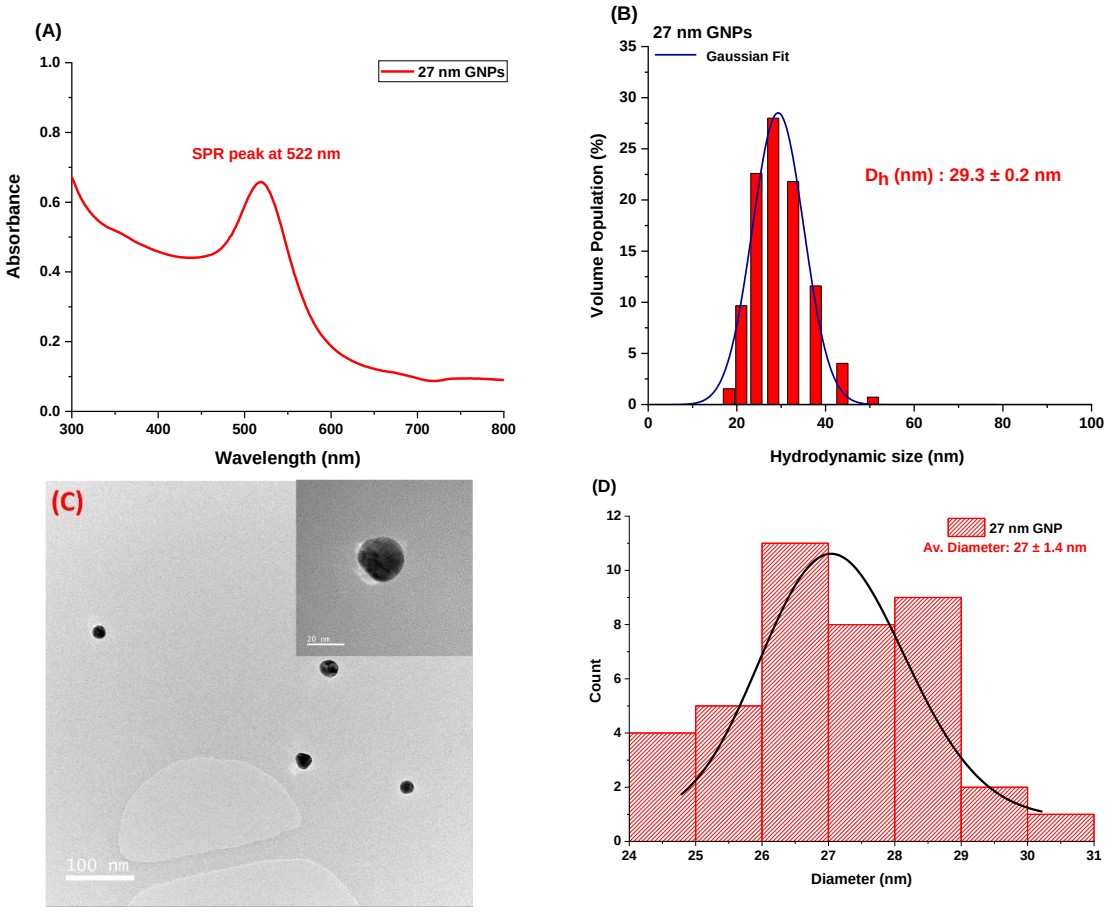

Figure S2. Characterisation of G27. (A) UV-vis absorption spectrum showing its SPR absorption peaking at ~522 nm, (B) D_h (volume population, fitted by Gaussian function) histogram showing a single Gaussian species with a D_h of ~29 nm; (C) A Typical TEM image (with higher magnification shown in the inset); (D) TEM measured GNP diameter histogram fitted by Gaussian function.

3. Synthesis of the LA-based Ligands[4, 5]

LA-EG_4-DiMan ligand was synthesised by copper-catalyzed "clicking" interactions between LA-EG_4- C≡CH and N_3-EG_2-DiMan as reported previously. All the glycans and linkers were synthesised in-house and purified using our established protocols.[5, 6]

(A) ^{1}H-NMR of LA-EG_4-DiMan in D_2O

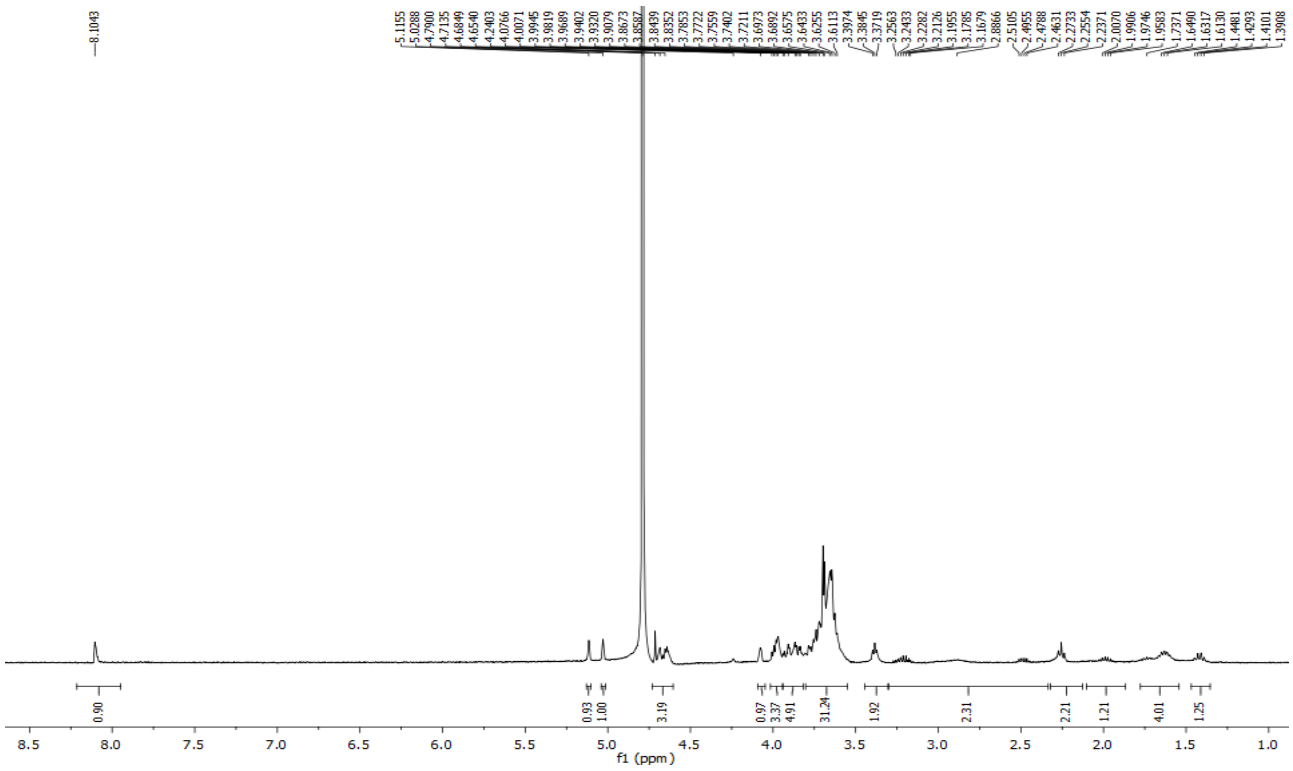

(B) ^{13}C-NMR of LA-EG_4-DiMan in D_2O

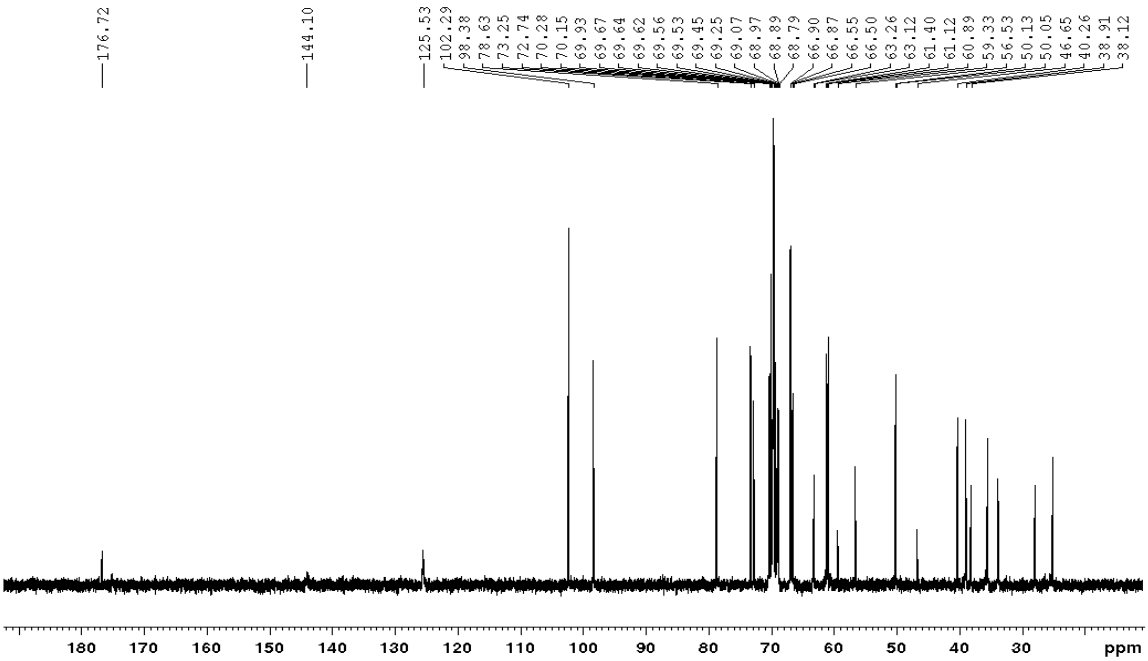

(C) LC-MS of LA-EG$_4$-DiMan

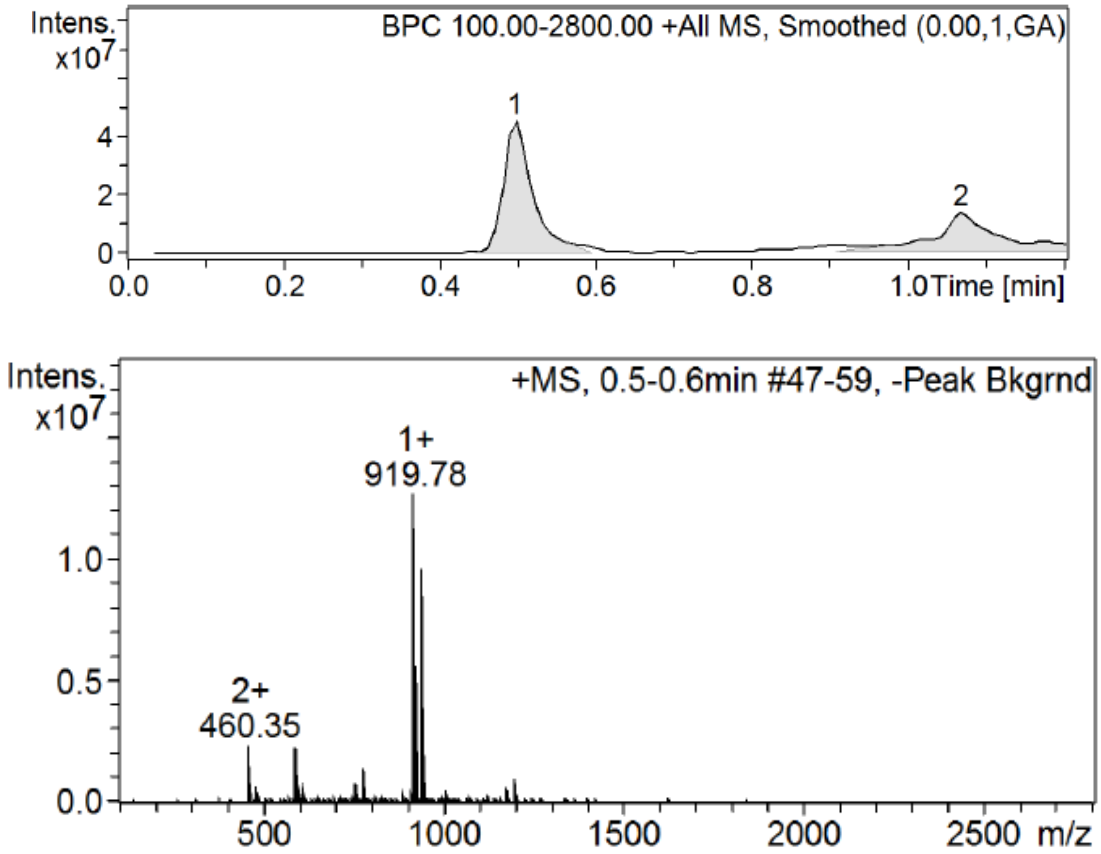

Figure S3. Spectroscopic characterisations of LA-EG$_4$-DiMan. (A) ^{1}H-NMR spectrum; (B) ^{13}C-NMR spectrum in D_2O; and (C) LC-MS analysis (chromatogram and molecular ion peaks).

3.2. Synthesis of LA-EG$_4$-OH

LA-EG$_4$-OH was synthesised by using Cu-catalyzed "click" reactions between LA-EG$_4$-C≡CH and N_3-EG$_2$-OH and purified using our established protocols.[4, 5]

(A) ^{1}H-NMR of LA-EG$_4$-OH in D$_2$O

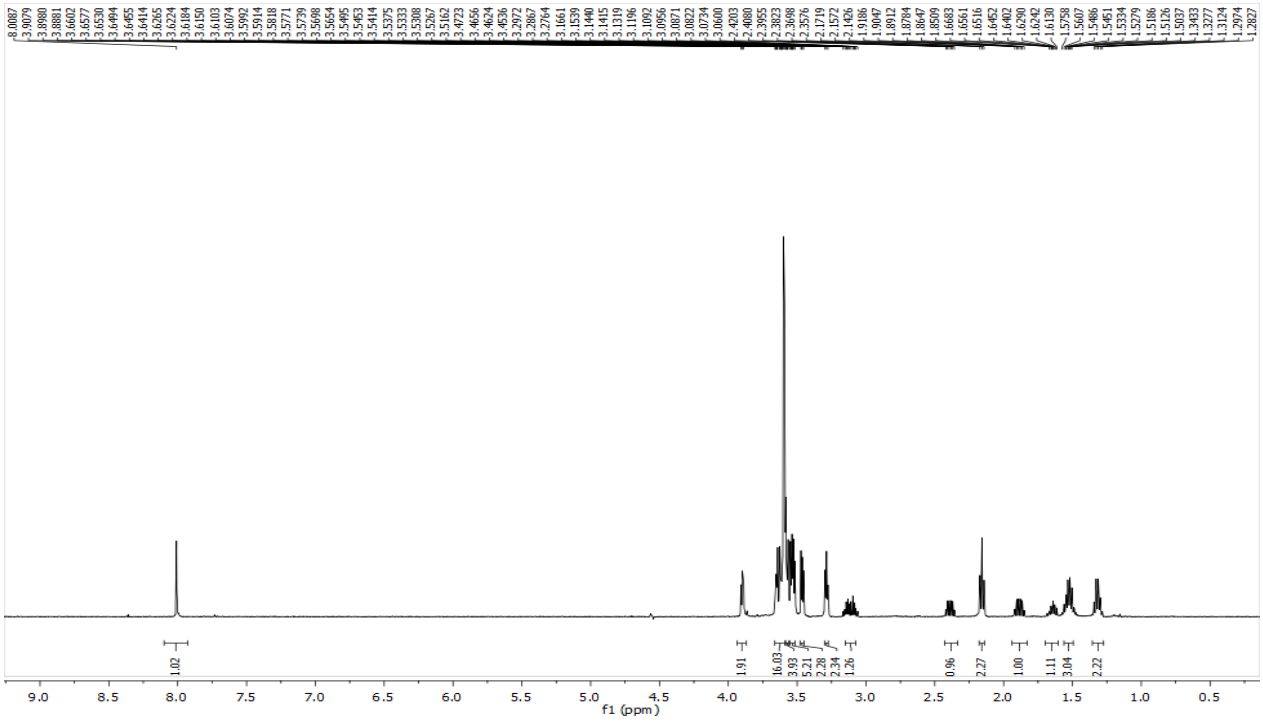

(B) ^{13}C-NMR of LA-EG$_4$-OH in D$_2$O

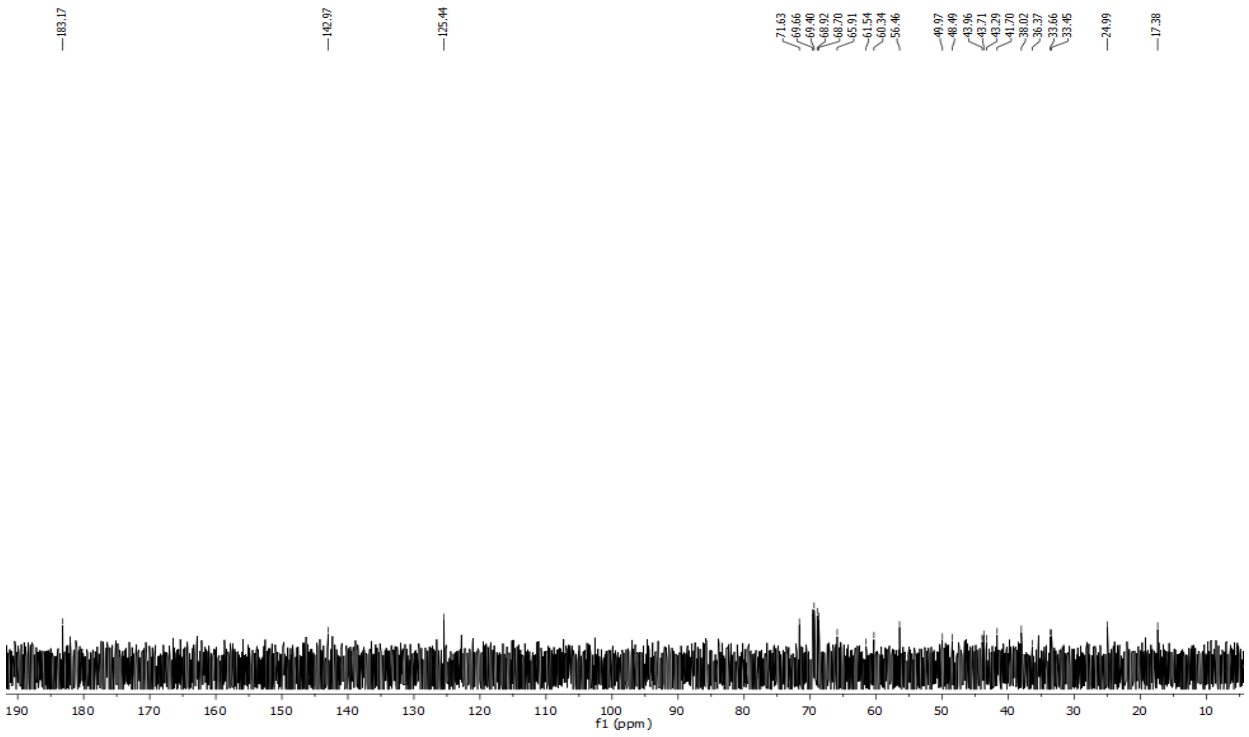

(C) LC-MS of LA-EG$_4$-OH

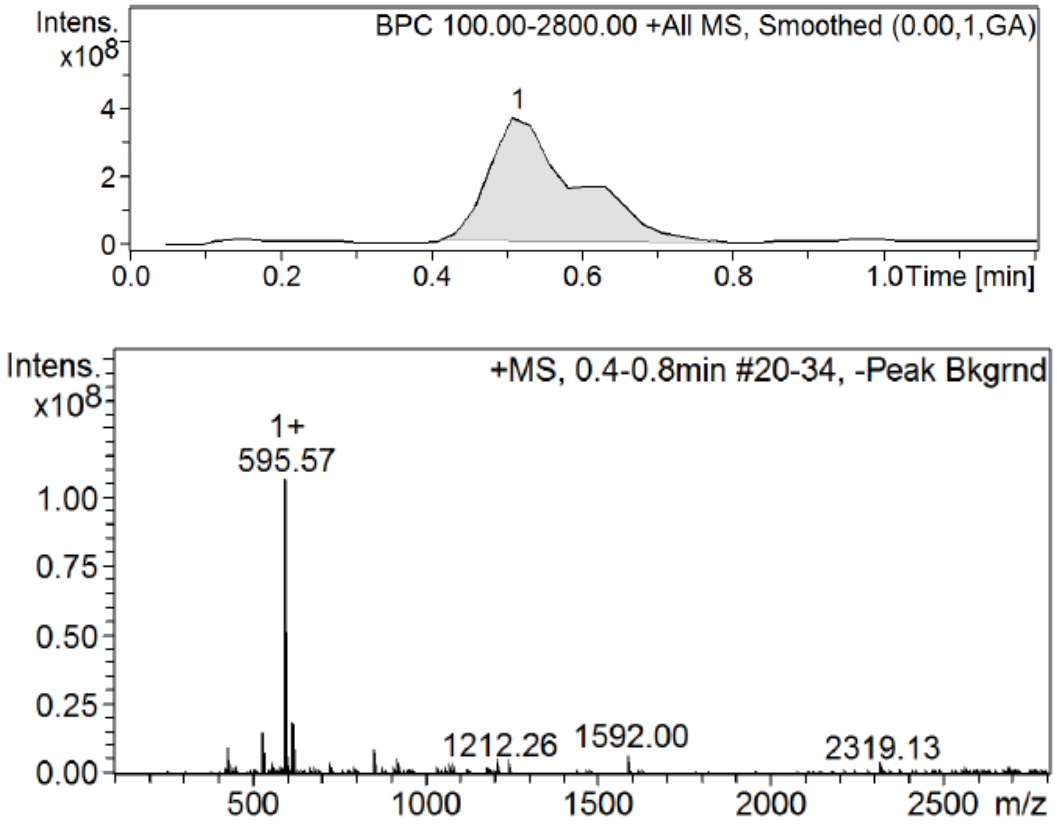

Figure S4. (A) ^{1}H-NMR spectrum in D_2O, (B) ^{13}C-NMR spectrum in D_2O, and (C) LC-MS spectrum (chromatogram and molecular ion peaks) of the final product, LA-EG$_4$-OH.

4. GNP-glycan Production and Characterisation[4, 5]

GNPs were conjugated with LA-glycan ligands via self-assembly in aqueous solutions. All GNP-glycans were highly stable and exhibited no changes in physical appearance or precipitation in buffers containing 200 mM NaCl, indicating that GNPs were covered with the desired LA-EG_4-based ligands. Their D_h histograms were shown in Figures S5-S7. G13-DiMan and G27-DiMan both exhibited a single D_h species of ~20 and ~29 nm, respectively, which were a few nm larger than the corresponding citrate stabilized parent GNPs, consistent with the Gx cores being coated with the LA-glycan ligands. Their UV-vis spectra overlaid well with the parent GNPs with no measurable red-shift and broadening of the SPR peaks, indicating the formation of stable, isolated single GNP-glycans.

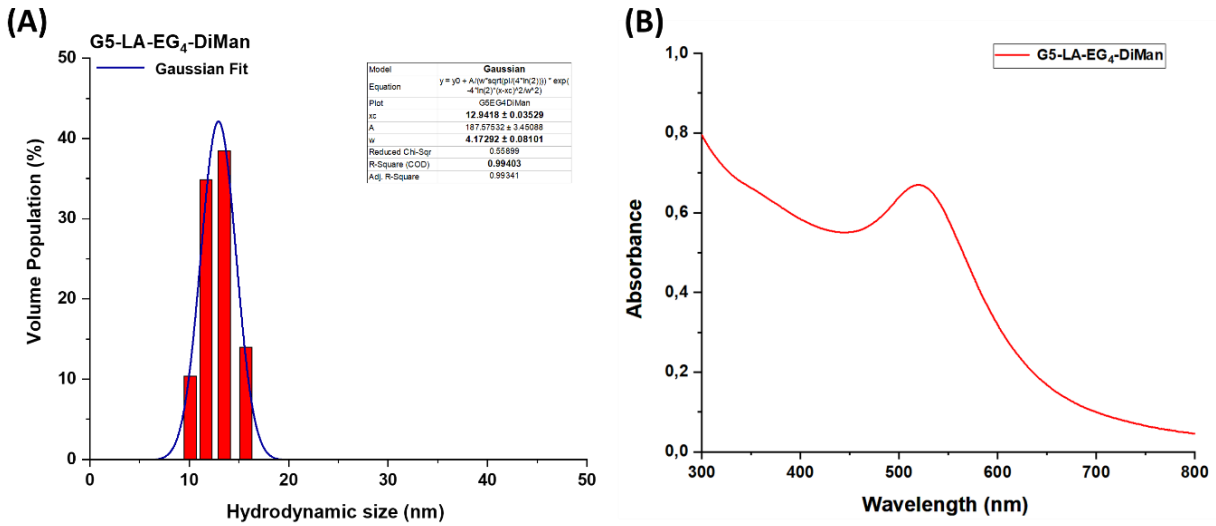

Figure S5. (A) The D_h histogram (volume population) for G5-DiMan fitted by Gaussian function (fitting parameters shown in the graph). (B) The UV-vis spectrum for G5-DiMan conjugate.

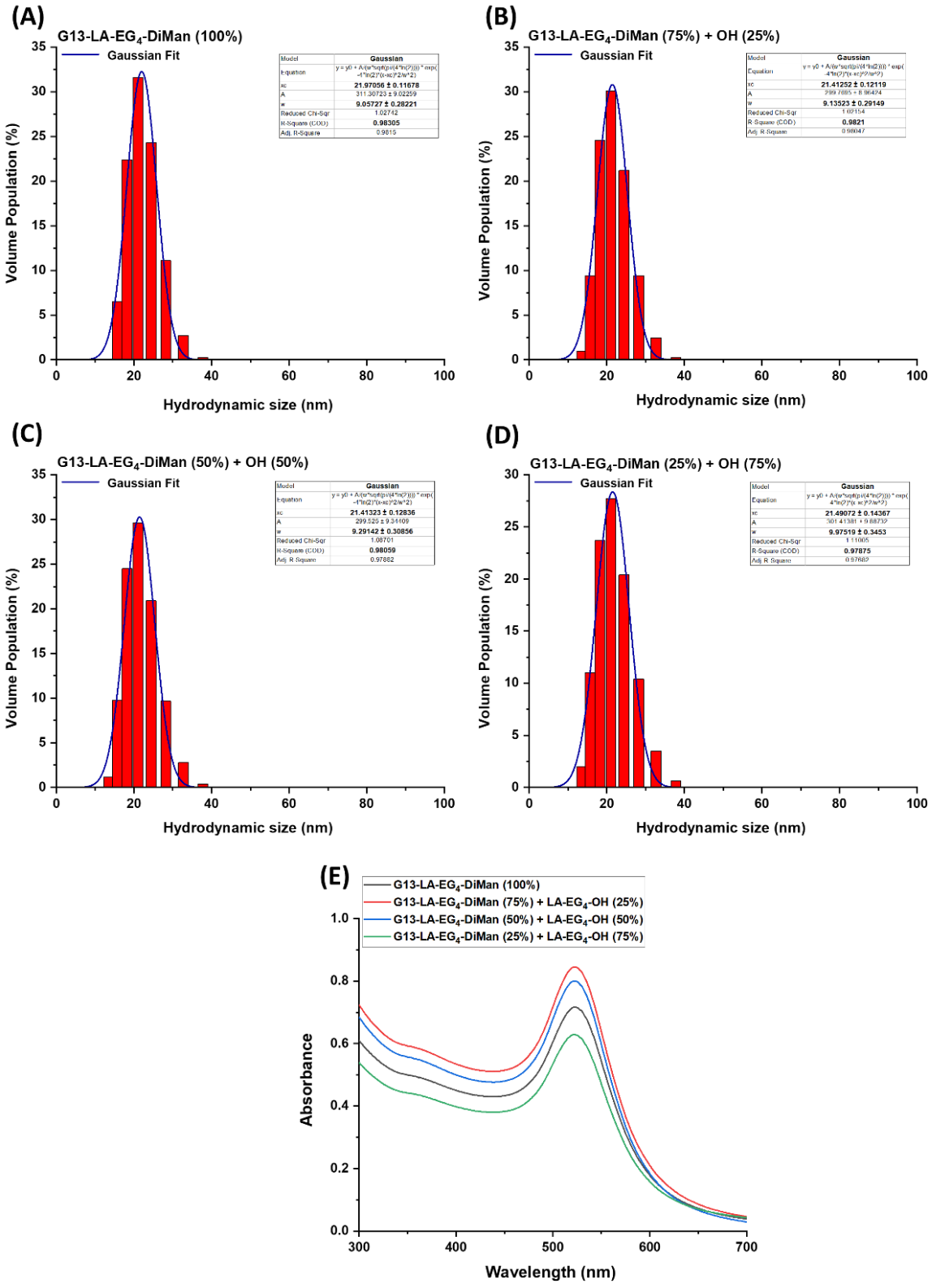

Figure S6. The D_h histograms (volume population) of (A) G13-DiMan (100%) and (B) G13-DiMan (75%); (C) G13-DiMan (50%); (D) G13-DiMan (25%) fitted Gaussian function (with fitting parameters shown in each graph); (E) The UV-vis spectra of G13-DiMan with glycan contents varied from 100% to 25%.

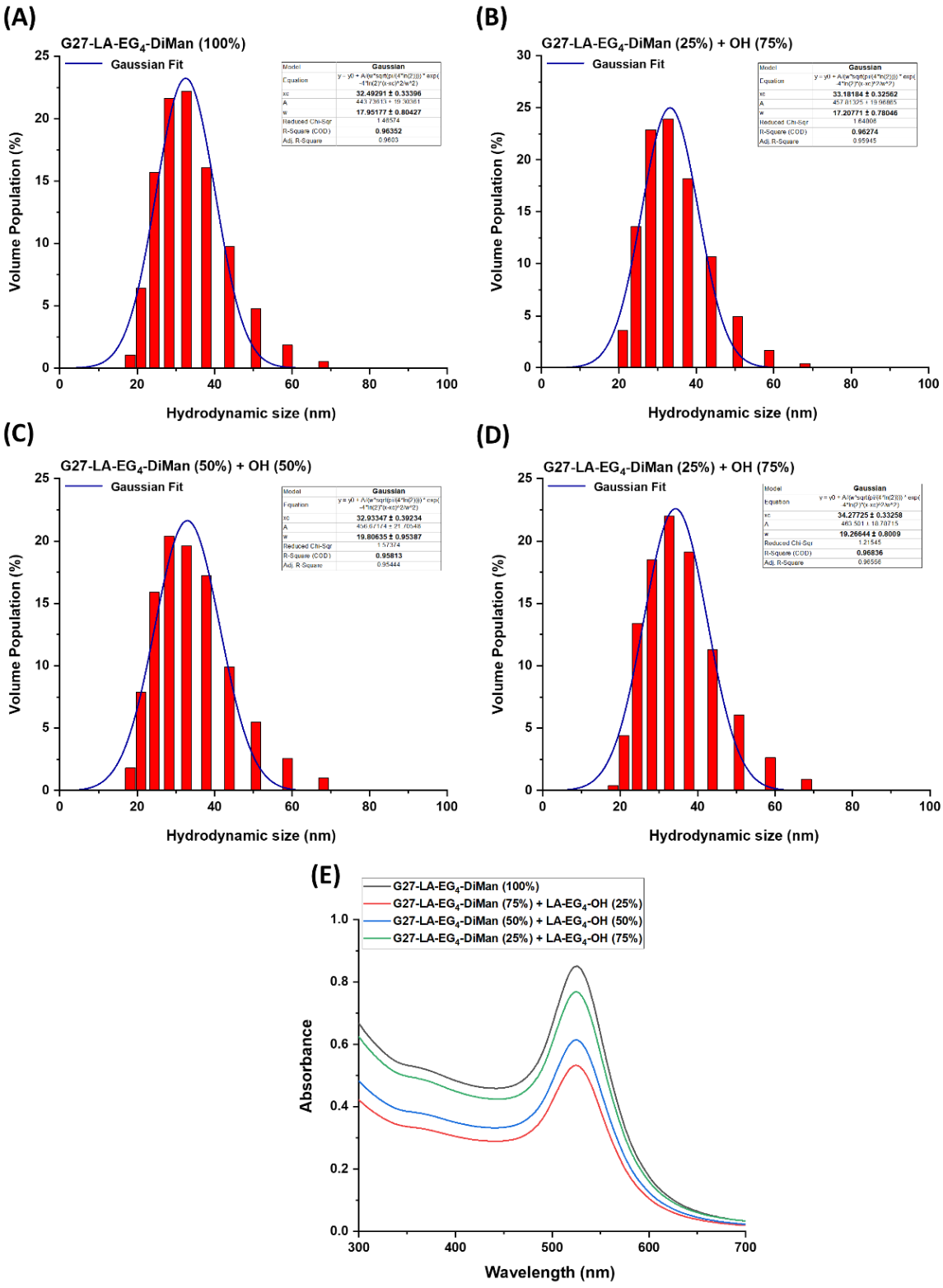

Figure S7. The D_h histograms (volume population) of (A) G27-DiMan (100%) and (B) G27-DiMan (75%); (C) G27-DiMan (50%); (D) G27-DiMan (25%) fitted Gaussian function (with fitting parameters shown in each graph); (E) The UV-vis spectra of G27-DiMan with glycan contents varied from 100% to 25%.

The GNP concentrations were calculated using the Beer-Lambert law from their SPR peak absorbance at ~520 nm. The extinction coefficients of different size GNPs were estimated from the extinction coefficient - diameter relationship (see Figure S8 below), giving extinction coefficients of 1.10×10^7, 2.32×10^8, and 2.39×10^9 $M^{-1}cm^{-1}$ for G5, G13, and G27, respectively.[4]

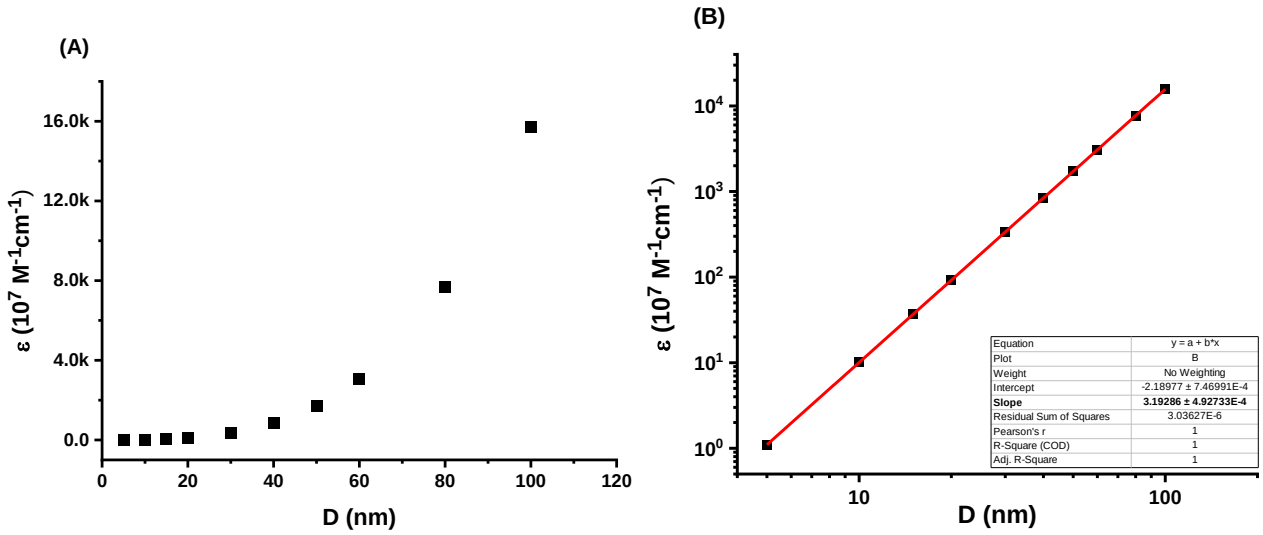

Figure S8. Plots of the GNP absorption coefficients (Ɛ) versus the GNP diameters with different sizes. The extinction coefficients of GNPs were obtained from the Sigma-Aldrich website.[7] (A) A linear-linear plot. (B) A $\log_{10}$-$\log_{10}$ plot reveals a good linear relationship ($R^2 = 1$) with a slope of 3.19, indicating that Ɛ increases linearly with the cubic diameter of GNPs ($D^{3.19}$). The extinction coefficients of GNPs scale linearly with roughly to their volumes.

5. Determination of Glycan Valency on GNP-glycans[4, 6]

The supernatants and washing though liquids collected from GNP-glycan purification were used to determine the amount of unbounded free ligands using the phenol-sulfuric acid method for carbohydrate quantification.[8] A calibration curve was first generated by using LA-EG_4-DiMan ligands. 80 µL of 5% phenol solution and 400 µL of concentrated H_2SO_4 were added to a series of glycan ligand solutions in H_2O (80 µL) containing 2.0-20 µg of LA-EG_4-DiMan ligand. The resulting mixtures were vortexed and then allowed to stand at RT for 30 mins. Their absorbance at 490 nm (A_{490}) were then recorded against a black water control. The A_{490}-concentration relationship was plotted by linear function to yield a calibration curve: $Y = (0.03415 \pm 0.0007)\ X$ (X in μM^{-1}).

The supernatants and washing-through filtrates were combined, freeze-dried, and then re-dissolved in 1.40 mL of pure water. 25 µL of each solution was diluted with water to a final volume of 125 µL. This solution was then mixed with 125 µL of 5% phenol and 625 µL of H_2SO_4 and incubated at RT for 30 mins. The absorbance of the mixture was recorded at 490 nm, and the dilution factors were corrected to calculate the total amount of unconjugated glycan ligand. The measurements were done in duplicate for each sample. The LA-glycan ligand amount difference between that added and that remained unbound after GNP conjugation was counted as LA-

glycan ligands that have bound to the GNP. The average number of LA-glycan ligands conjugated to each GNP were given in Table S1 below.

Table S1. Summary of the average number of LA-glycan ligands conjugated to each GNP.

GNP-glycan conjugates	**Glycan valency per GNP**
G5-DiMan (100%)	730 ± 52
G13-DiMan (100%)	2200 ± 172
G13-DiMan (75%)	1640 ± 137
G13-DiMan (50%)	1040 ± 88
G13-DiMan (25%)	520 ± 47
G27-DiMan (100%)	6290 ± 440
G27-DiMan (75%)	4870 ± 332
G27-DiMan (50%)	3150 ± 247
G27-DiMan (25%)	1540 ± 122

5.1. Calculation of the average inter-glycan distance on GNPs [4, 6]

The average inter-glycan distance (*X*) of Gx-DiMan (x = 5, 13 or 27) was calculated from their D_h and glycan valency, based on the method reported by Hill *et al.*[9] For a GNP-glycan with a hydrodynamic radius of *r* (*r* = 1/2 D_h) covered with N ligand, the footprint of each ligand (*k*) on the GNP surface is:

$$k = \frac{4\pi r^2}{N}$$

Where *r* is hydrodynamic radius (*r* = 1/2 D_h). Given D_h = 12.9, 21.9 and 32.4 nm for G5-, G13- and G27-DiMan, thus *r* = 6.45 nm for G5-DiMan, 10.95 nm for G13-DiMan, and 16.2 nm for G27-DiMan, respectively. The average deflection angle of each ligand on the GNP surface (θ, in degrees) was calculated *via* the equation below.

$$\theta = \frac{2 \times 180\, x \sqrt{\frac{k}{\pi}}}{r\pi}$$

The estimated θ values for Gx-DiMan (x = 5, N = 730; x = 13, N = 2200; and x = 27, N = 6290) were 8.48°, 4.88°, and 2.89°, respectively. Using these data, the average inter-glycan distance on Gx-DiMan (*X*) was then calculated via the following equation.

$$X = 2\,r\,\sin\left(\frac{\theta}{2}\right)$$

Using these data, the average inter-glycan distances were estimated as ~0.95, ~0.93, and ~0.80 nm for G5-DiMan, G13-DiMan and G27-DiMan, respectively. These values matches well with the most of inter-glycan sequon spaces (*e.g.* 0.7−1.3 nm) found on the HIV surface trimeric glycoprotein gp160.[10]

6. Protein Production and Characterisation

6.1. Wild-Type DC-SIGN and DC-SIGNR[4, 6]

DC-SIGN/R were expressed from *E. coli.* and purified by sepharose-mannose affinity chromatography as described previously.[4, 6] Their concentrations were determined by their absorbance at 280 nm using a monomer extinction coefficient of 70 400 and 60 890 M^{-1} cm^{-1} for DC-SIGN and DC-SIGNR, respectively. The proteins were characterised by high-resolution mass spectrometry (HR-MS, Figure S9) and DLS (Figure S10). The calculated molecular weights of DC-SIGN and DC-SIGNR based on amino acid sequences are 39197.22 and 37478.99, and found 39201.61, and 37470.40, respectively.

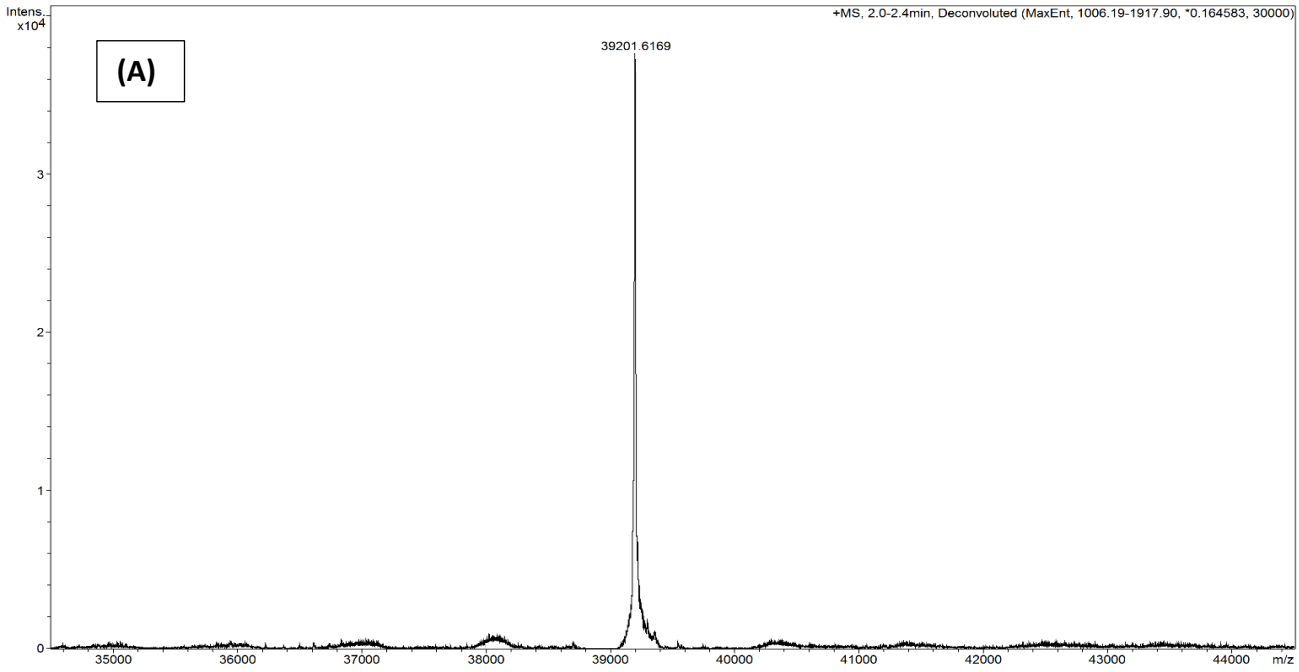

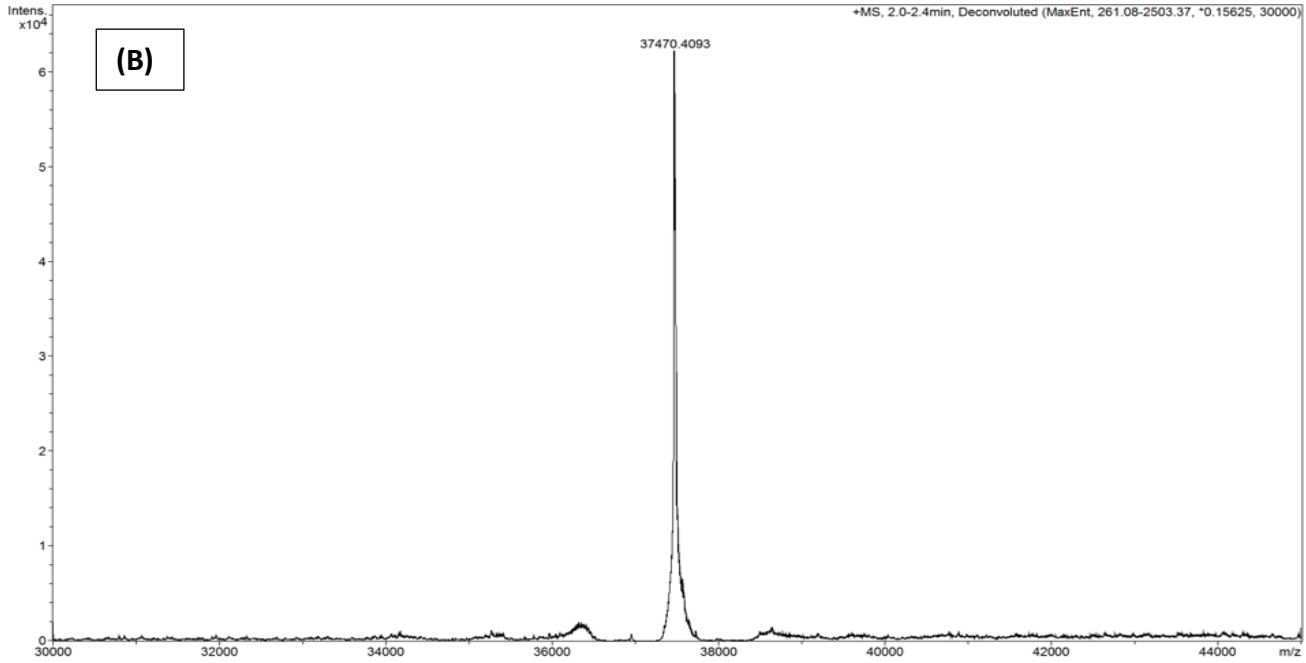

Figure S9. HR-MS spectra of (A) wild-type DC-SIGN (DC020) and (B) DC-SIGNR (DSR034).

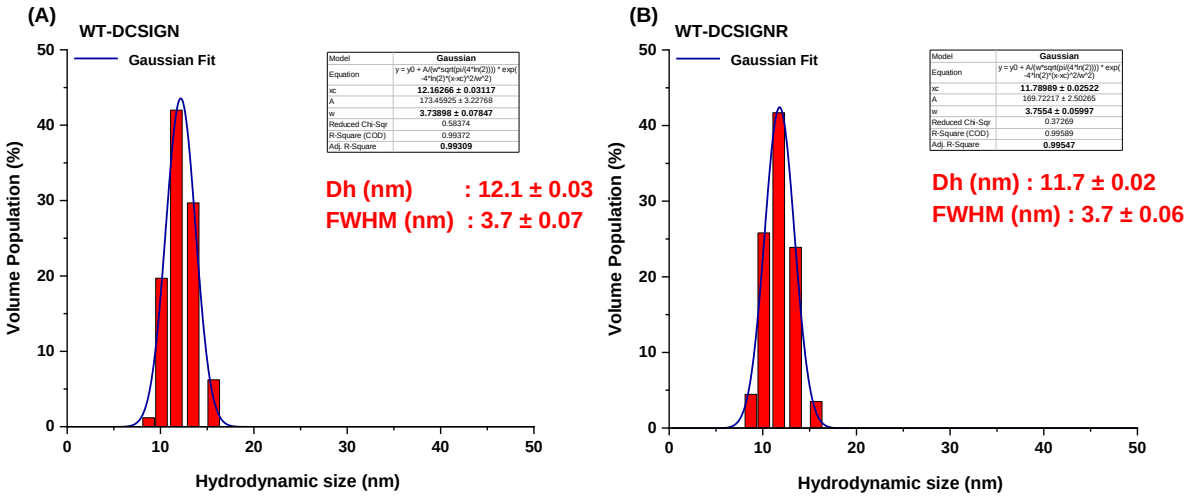

Figure S10. The D_h (volume population) histograms for (A) wild-type DC-SIGN; (B) wild-type DC-SIGNR fitted by Gaussian function with fitting parameters shown in each graph.

6.2. Production and Characterisation of Atto-643 labelled DC-SIGN and DC-SIGNR[4, 6]

The production, site-specific Atto-643 labelling and purification of labelled lectins were performed on mutant lections with a site-specific cysteine mutation at Q274C in DC-SIGN and R287C in DC-SIGNR as described previously.[4, 6] The successful Atto-643 labelling was confirmed from an increase of molecular weight of ~882 Da, corresponding to the MW of Atto-643 dye, as observed in the HR-MS spectra. The labelling efficiency was calculated from the abundance of the labelled peak area to that of the total lectins (labelled + unlabelled), giving ~82% and ~90% per monomer for DC-SIGN and DC-SIGNR, respectively (Figure S11).

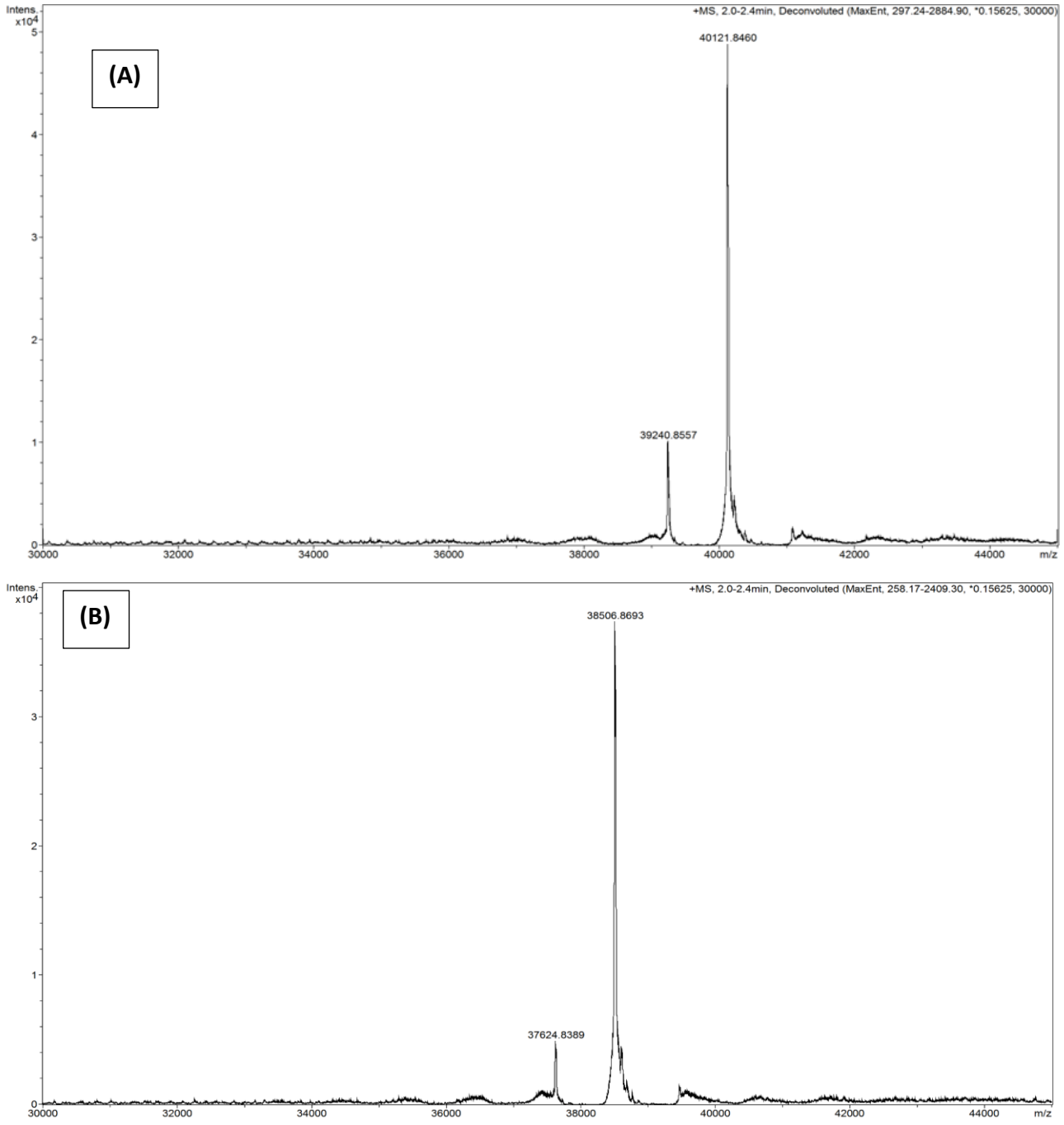

Figure S11. HR-MS spectra of (A) DC-SIGN-Atto 643 (DC020 Q274C-Atto 643) and (B) DC-SIGNR-Atto 643 (DSR034 R287C-Atto 643).

7. Fluorescence Spectra of GNP-glycans binding with Atto-643 labelled DC-SIGN/R

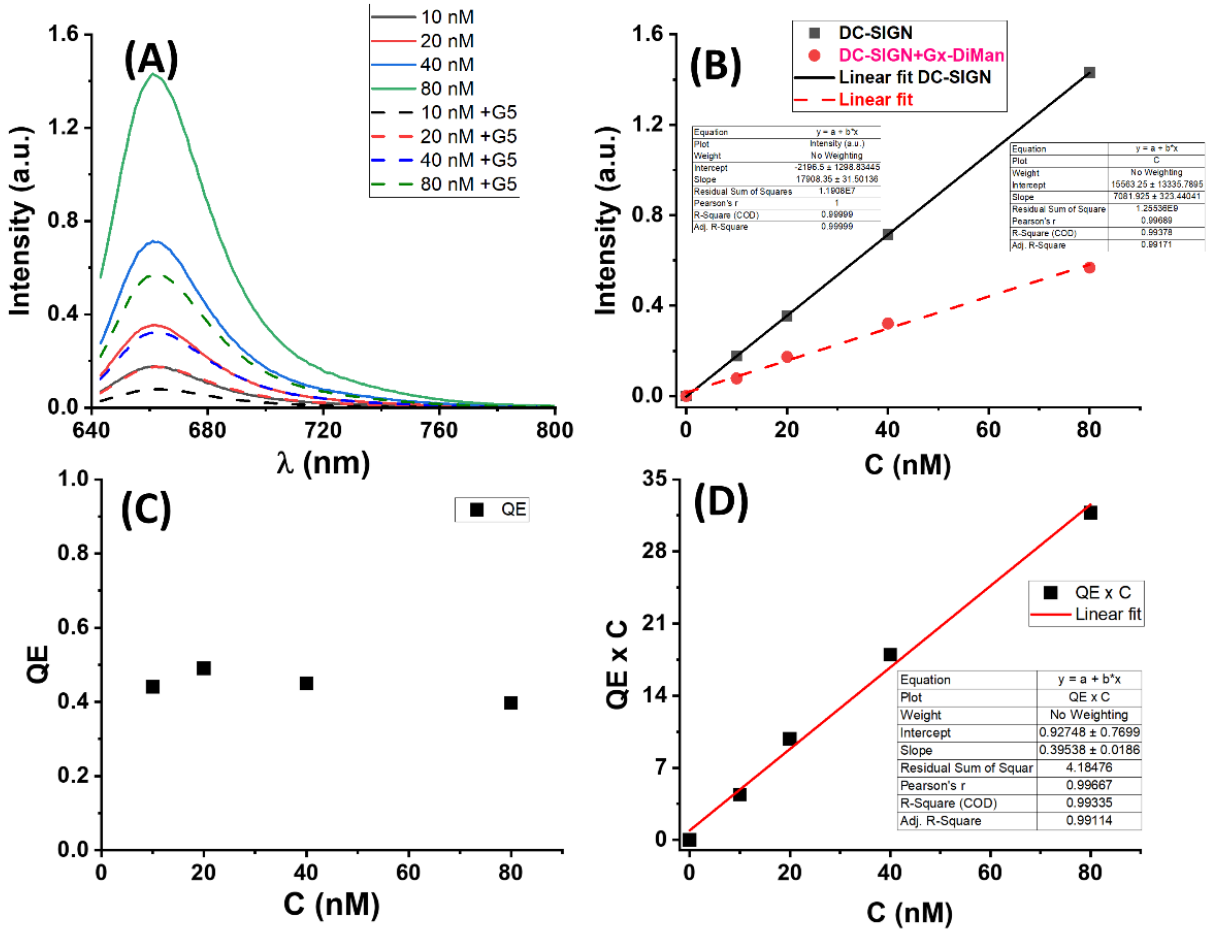

Figure S12. (A) Fluorescence spectra of varying concentration (*C*) Atto-643 labelled DC-SIGN recorded without (solid lines) and with 10 nM G5-DiMan. (B) Fluorescence intensity *vs.* concentration plots for DC-SIGN only (black squares) and DC-SIGN + G5-DiMan (red dots) showing excellent linear relationships (R^2 > 0.99). (C) A plot of QE *vs.* DC-SIGN concentration for G5-DiMan quenching of DC-SIGN fluorescence showing the QE stays almost constant over this range. (D) A plot of (QE × *C*) *vs.* *C* plot fitted by linear relationship (R^2 > 0.99) for G5-DiMan binding with DC-SIGN, yielding an average QE of 0.395 ± 0.019.

7.1. Fluorescence Spectra of DC-SIGN/R and G5-Glycans binding with DC-SIGN/R

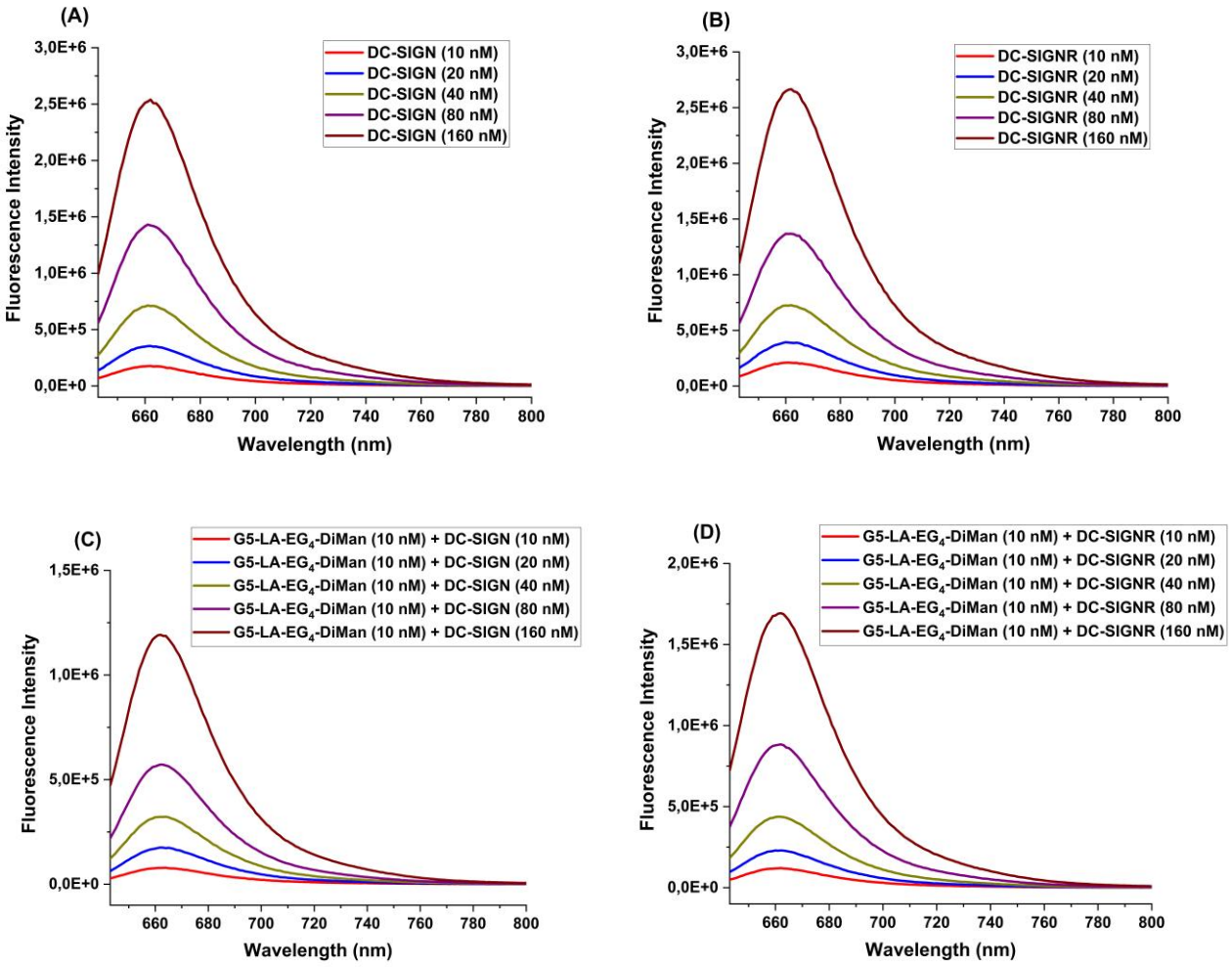

Figure S13. The fluorescence spectra of (A) DC-SIGN; (B) DC-SIGN/R; (C) G5-DiMan + DC-SIGN; (D) G5-DiMan + DC-SIGNR. Each concentration was done in duplicate and their average fluorescence spectra was used for QE calculation.

7.2. Fluorescence Spectra for G13-Glycans binding with DC-SIGN/R

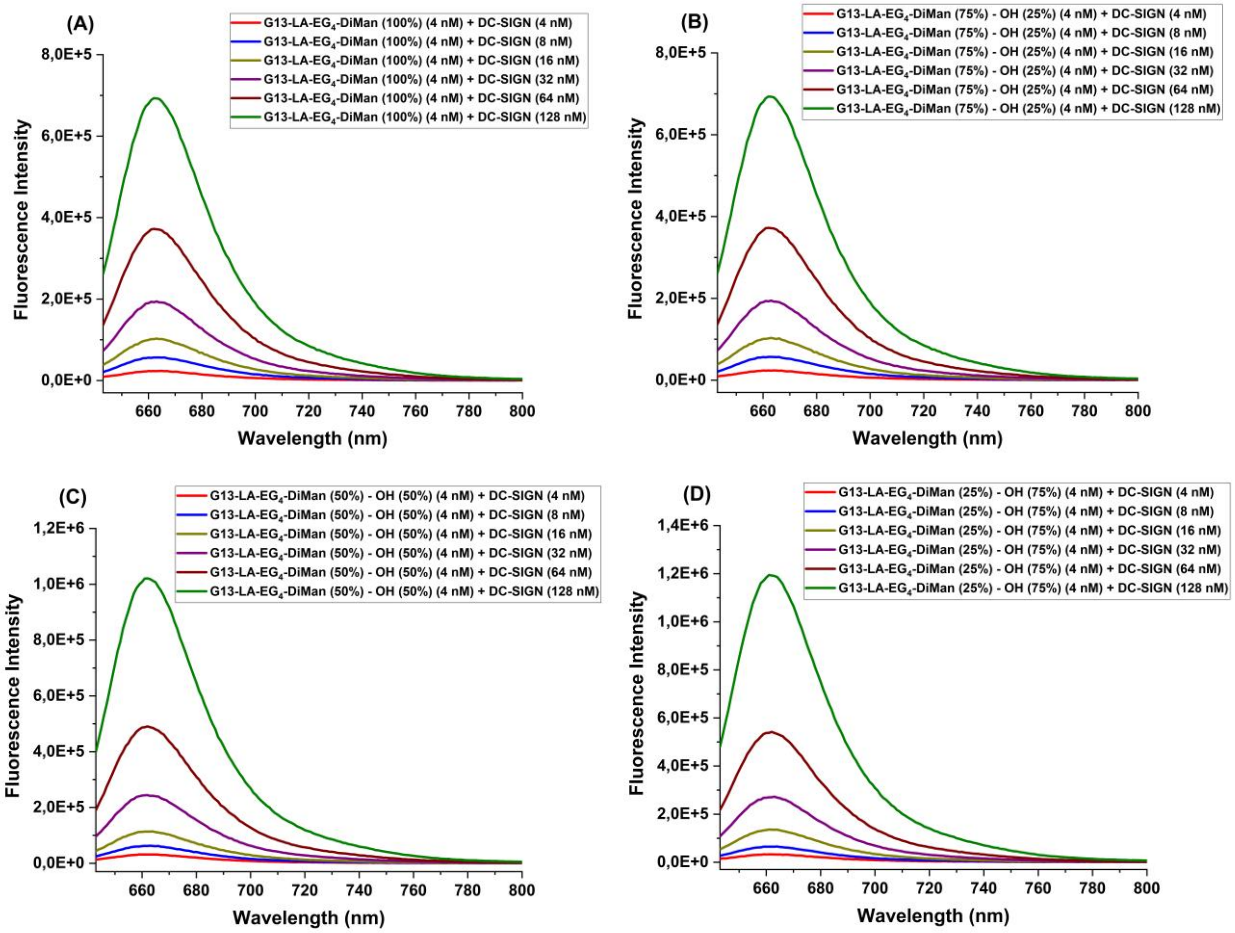

Figure S14. The fluorescence spectra of DC-SIGN binding with (A) G13-DiMan(100%); (B) G13-DiMan(75%)-LA-OH(25%); (C) G13-DiMan(50%)-LA-OH(50%); and (D) G13-DiMan(25%)-LA-OH(75%). Each concentration was done in duplicate and their average fluorescence spectra was used for QE calculation.

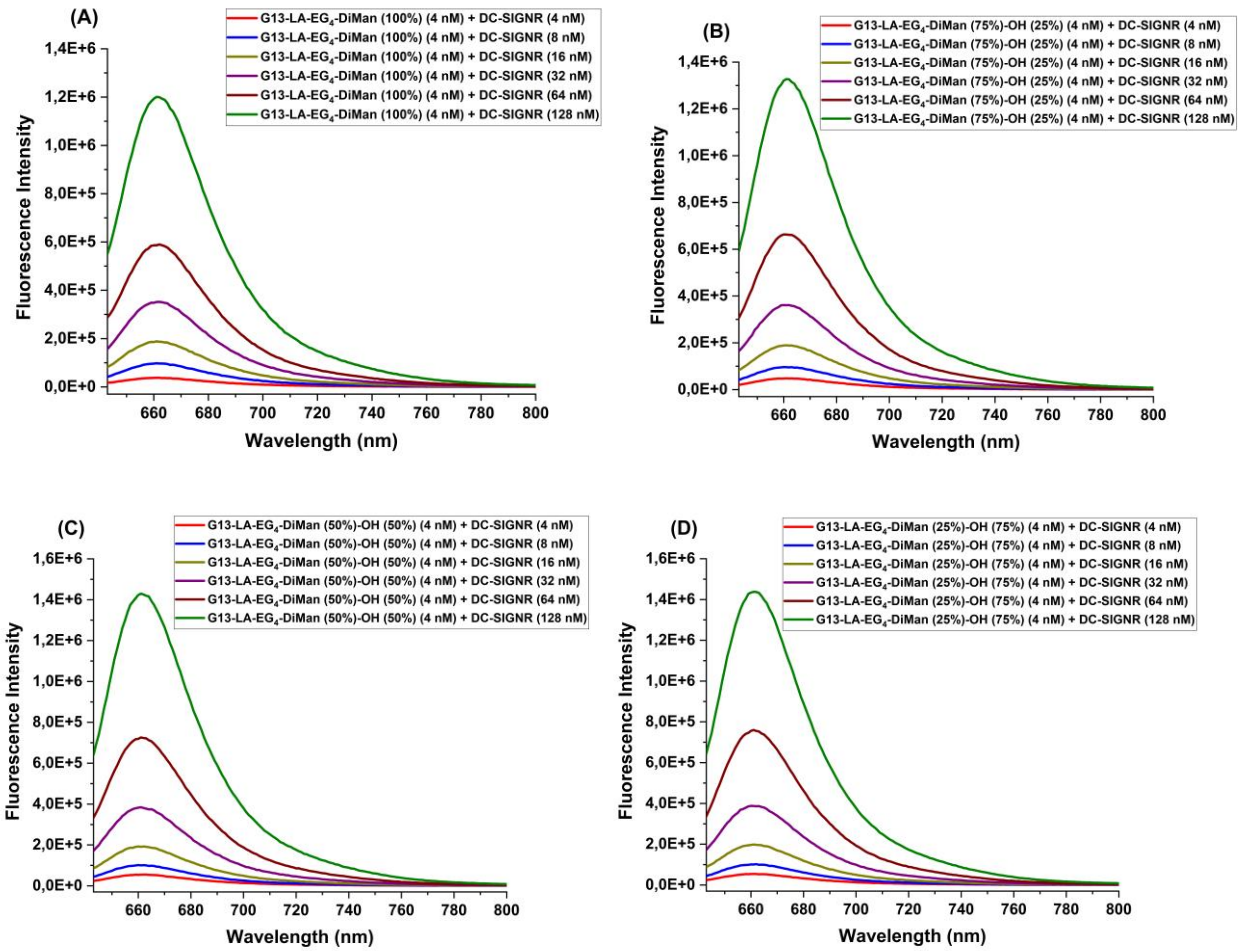

Figure S15. The fluorescence spectra of DC-SIGNR binding with (A) G13-DiMan (100%); (B) G13-DiMan (75%)-LA-OH(25%); (C) G13-DiMan(50%)-LA-OH(50%); and (D) G13-DiMan(25%)-LA-OH(75%). Each concentration was done in duplicate and their average fluorescence spectra was used for QE calculation.

7.3. Fluorescence Spectra for G27-Glycans binding with DC-SIGN/R

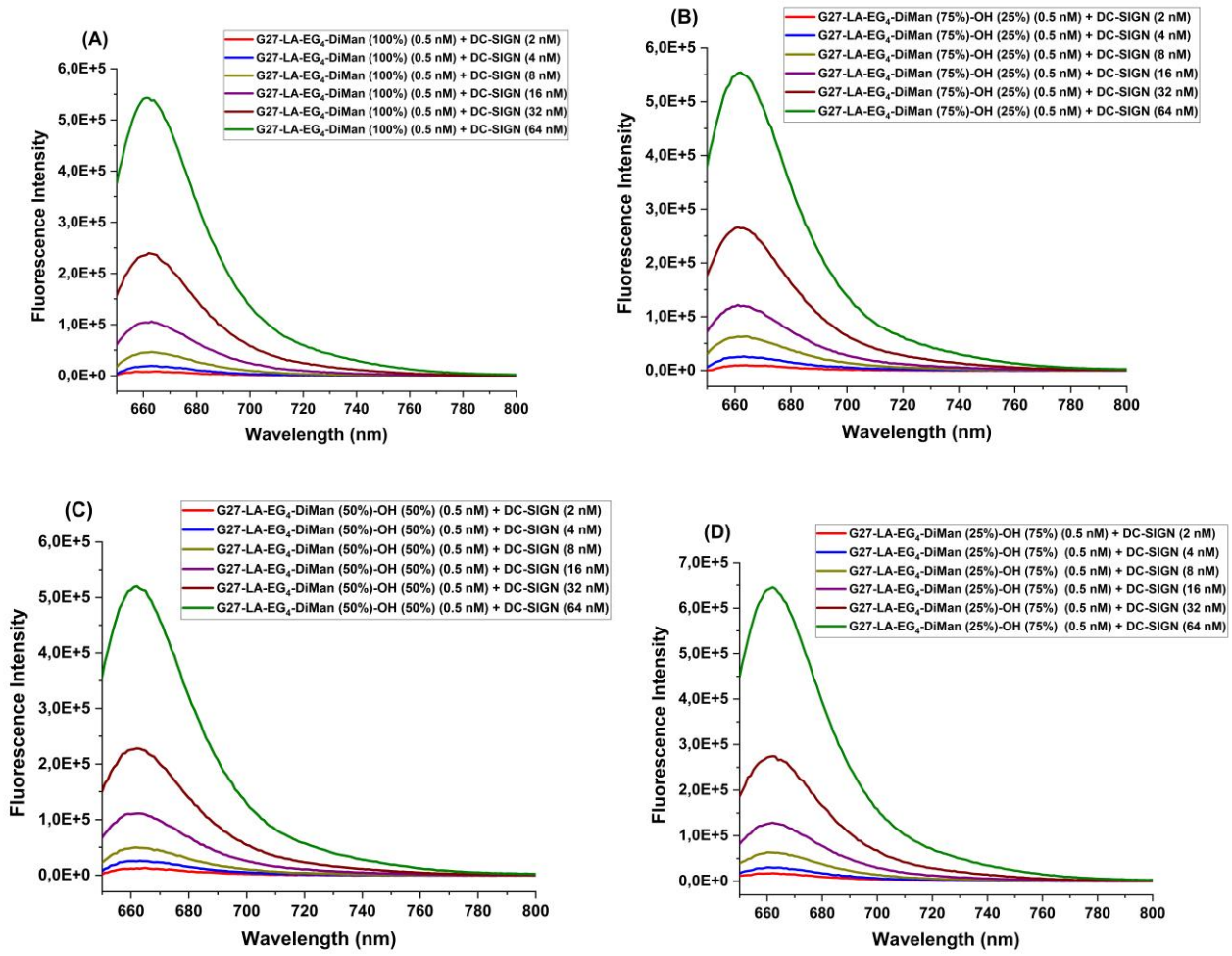

Figure S16. The fluorescence spectra of DC-SIGN binding with (A) G27-DiMan (100%); (B) G27-DiMan(75%)-LA-OH(25%); (C) G27-DiMan(50%)-LA-OH(50%); and (D) G27-DiMan(25%)-LA-OH(75%). Each concentration was done in duplicate and their average fluorescence spectra was used to calculate QE.

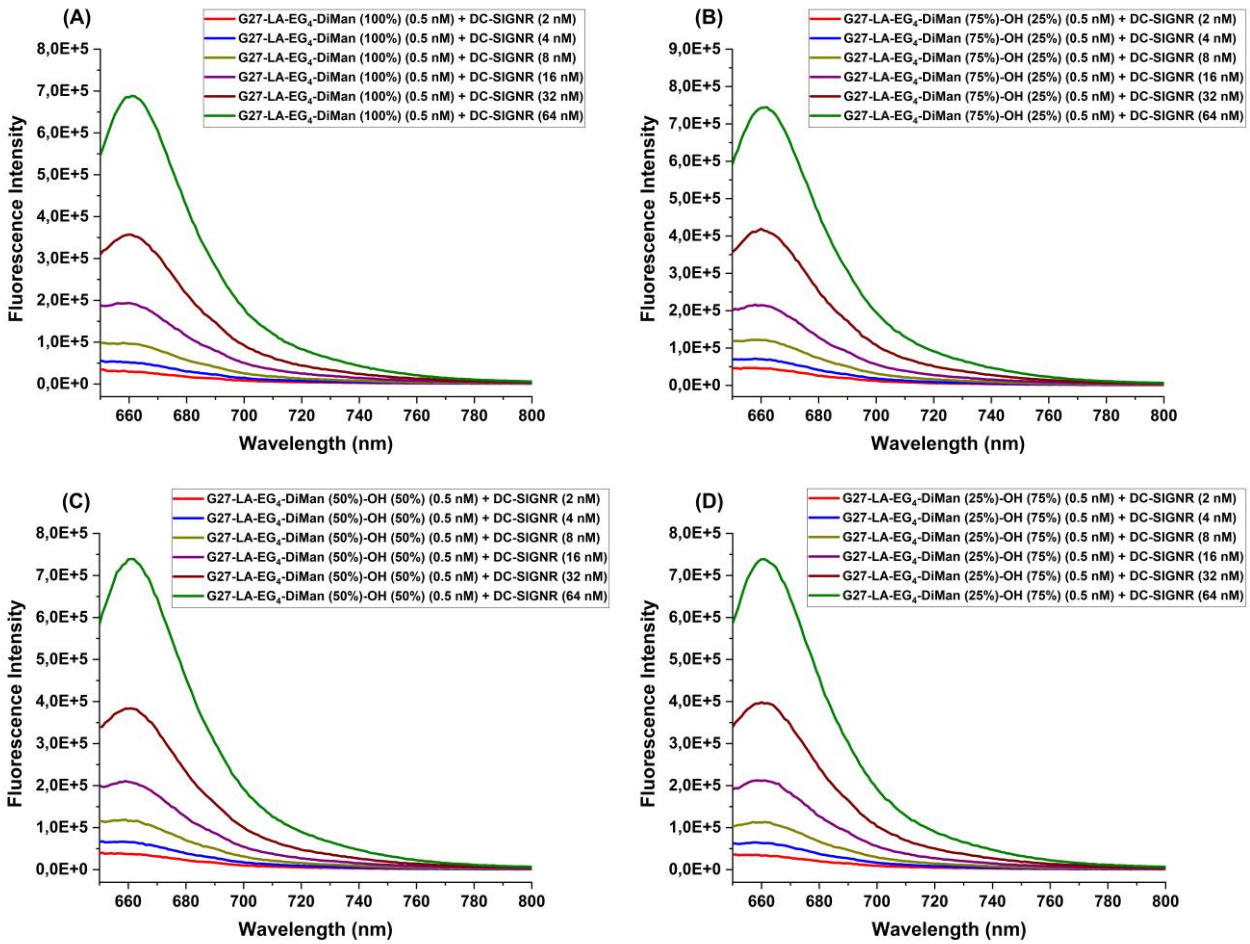

Figure S17. The fluorescence spectra of DC-SIGNR binding with (A) G27-DiMan (100%); (B) G27-DiMan(75%)-LA-OH(25%); (C) G27-DiMan(50%)-LA-OH(50%); and (D) G27-DiMan(25%)-LA-OH(75%). Each concentration was done in duplicate and their average fluorescence spectra was used to calculate QE.

7.4. (QE × C) *vs. C* Plots and linear fits for Gx-glycans binding with DC-SIGN/R

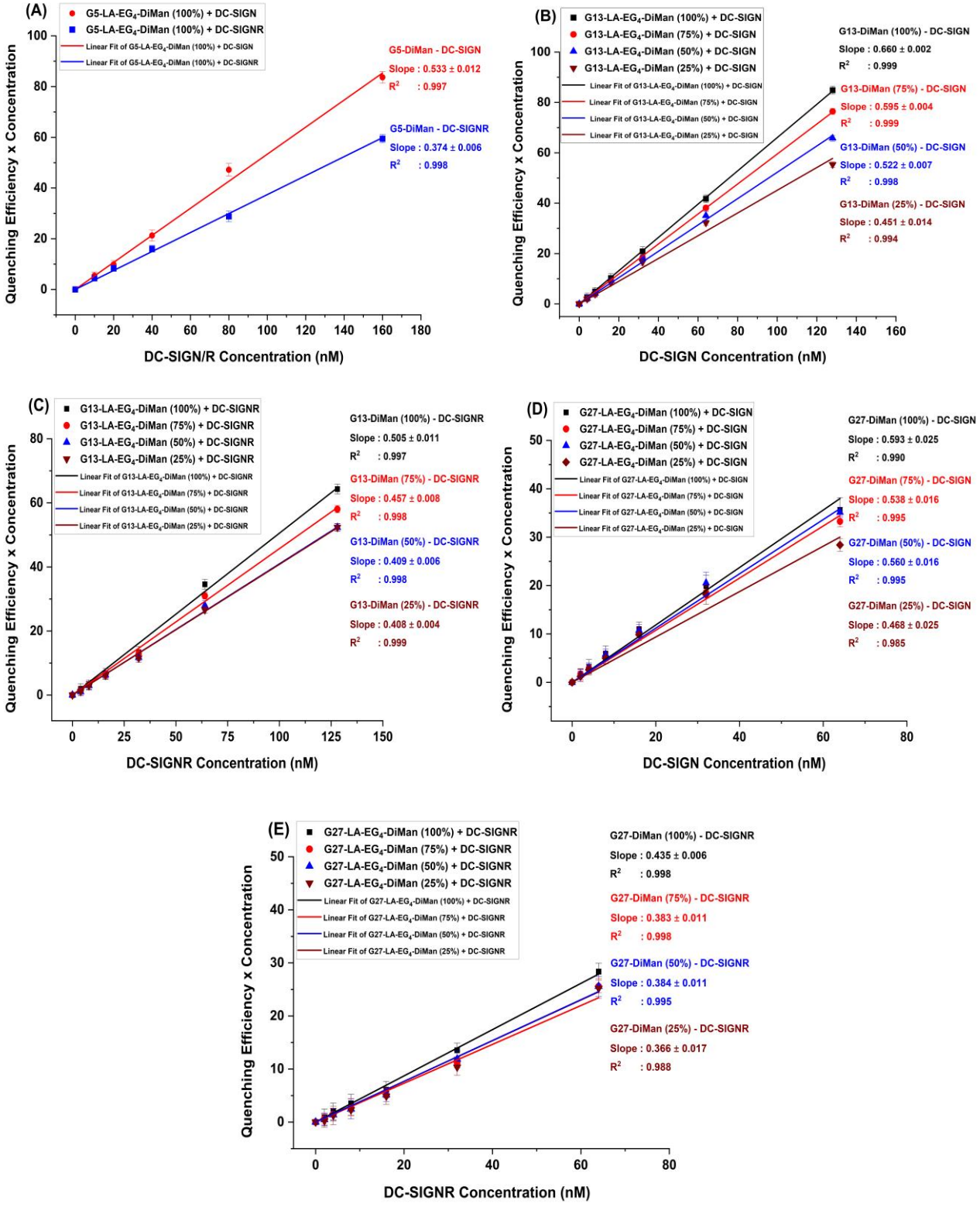

Figure S18. The (QE × *C*) *versus C* plots of (A) G5-DiMan + DC-SIGN or DC-SIGNR; (B) G13-DiMan + DC-SIGN; (C) G13-DiMan + DC-SIGNR; (D) G27-DiMan + DC-SIGN; and (E) G27-DiMan + DC-SIGNR.

7.5. Mannose Competition Studies

In order to verify whether the fluorescence quenching observed was due to the specific binding between GNP-glycans and DC-SIGN/R, mannose competition studies were performed by adding increasing concentrations of free mannose, which could compete with GNP-glycans in binding to DC-SIGN/R. Also, GNPs coated with LA-EG_4-OH ligands lacking the terminal glycans were used to quantify the non-specific quenching obtained from the inner filter effects of GNPs. Because the absorption of the excitation and emission light by GNPs would decrease the fluorescence intensity of the proteins in the absence of any specific binding, this would yield over-estimation of the actual quenching efficiency induced by binding. Adding free mannose to compete with GNP-glycans for DC-SIGN/R binding would result in reduced fluorescence quenching, and thus recovery of the protein fluorescence. The experiments were done using fixed concentrations of the GNP-glycans and labelled DC-SIGN/R (protein: GNP ratios for G5-, G13-, and G27-DiMan were 5, 10, and 60, respectively) with increasing concentrations of mannose. Figure S19 below shows the fluorescence spectra of Gx-EG_4-DiMan (x= 5, 13, and 27) and DC-SIGN/R mixture in the presence of varying free mannose concentration. As a control, the fluorescence spectra of the control Gx-EG_4-OH (x= 5, 13, and 27) and DC-SIGN/R mixture in the presence of different mannose competitor were also recorded and shown in Figure S20 below. An increase in the fluorescence intensity for both proteins was observed with the increasing mannose concentrations. This confirmed that free mannose effectively competed with GNP-DiMan in binding DC-SIGN/R, and the observed fluorescence quenching for GNP-DiMan and DC-SIGN/R samples are truly due to the specific lectin-glycan interactions. To obtain the true quenching data arising from specific binding, the results observed for the GNP-glycans were subtracted by those obtained from the GNP-EG_4-OH controls to correct the contribution from GNP's inner filter effect. The fluorescence recovery was then quantified by the fluorescence intensity ratio of GNP-glycan + DC-SIGN/R with mannose (defined as I) to that without mannose (defined as I_0). The fluorescence recovery ratio (I/I_0-1) versus mannose concentrations plots were then fitted by the Hill equation to derive the maximal fluorescence recovery ratio (Vmax), mannose concentration giving 50% of Vmax (K), and competition coefficient (n) values. Figure S21 shows the resulting fluorescence recovery plots as a function of mannose concentration for each GNP-DiMan with DC-SIGN/R. Table S3 below summarizes the fitting parameters of mannose competition assays obtained from Figure S21.

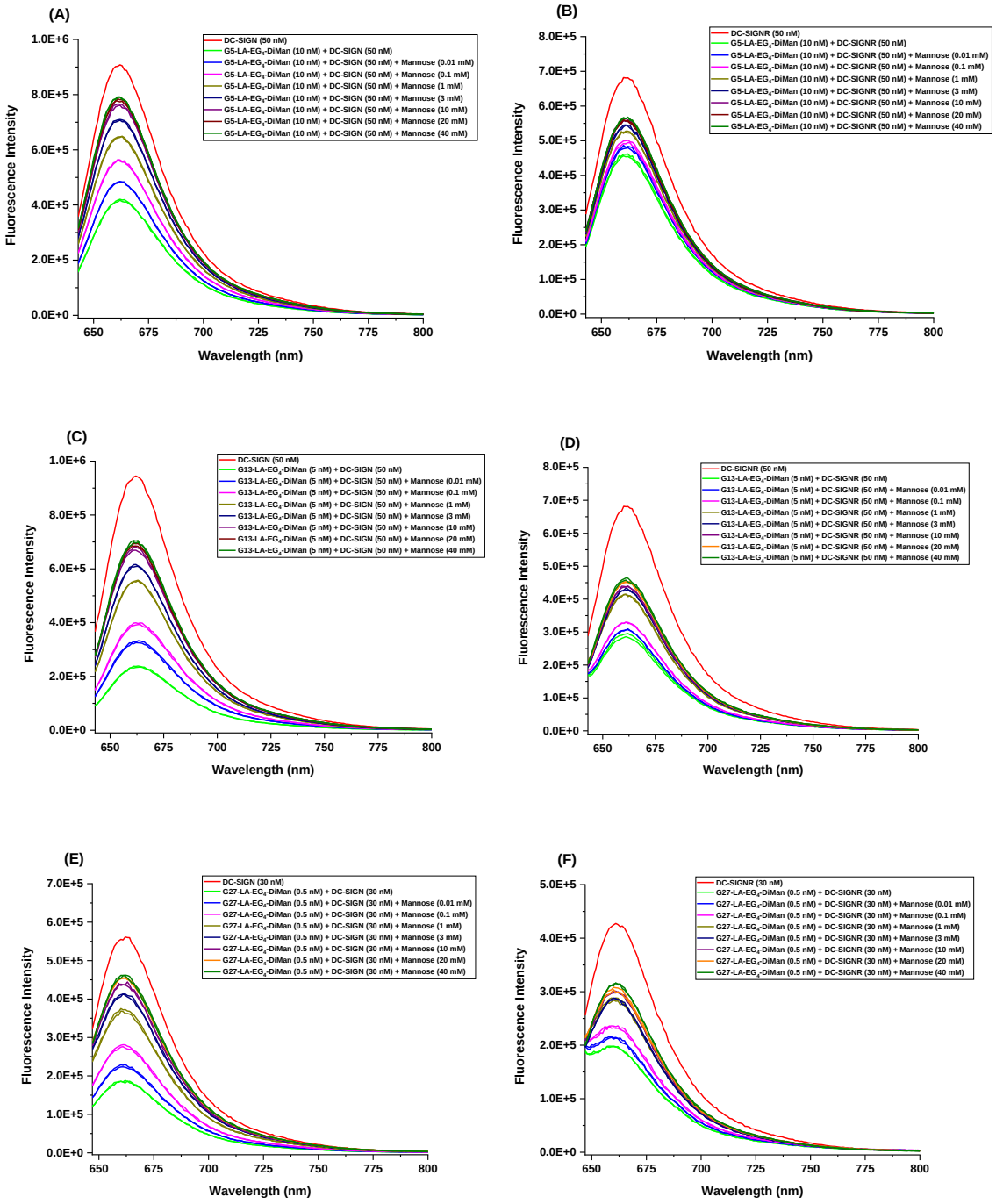

Figure S19. The fluorescence spectra of Gx-DiMan + DC-SIGN or DC-SIGNR upon the addition of an increasing concentration of free mannose. (A) G5-DiMan + DC-SIGN; (B) G5-DiMan + DC-SIGNR; (C) G13-DiMan + DC-SIGN; (D) G13-DiMan + DC-SIGNR; (E) G27-DiMan + DC-SIGN; and (F) G27-DiMan + DC-SIGNR. Each Gx-DiMan + DC-SIGN/R sample was measured in duplicate.

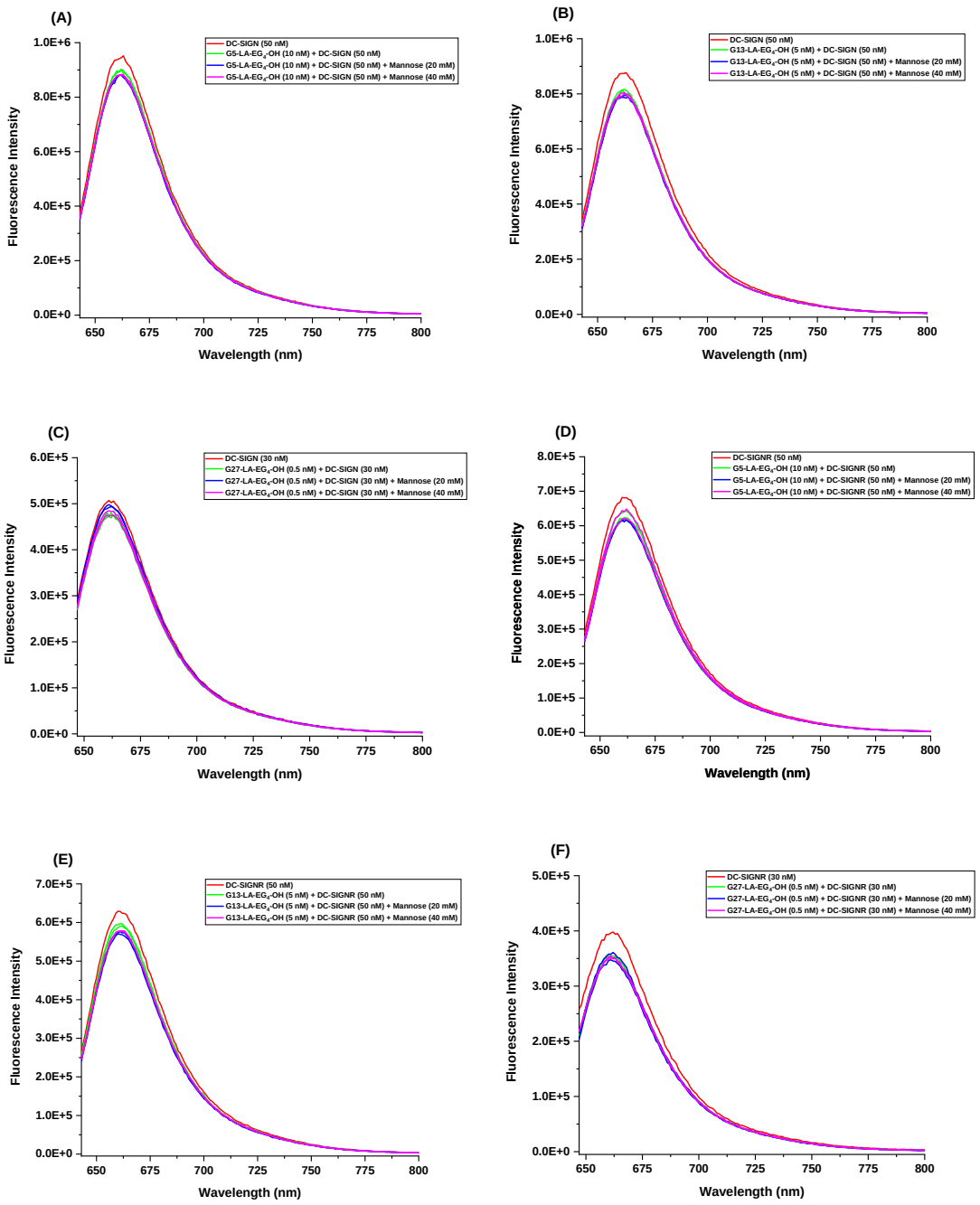

Figure S20. The fluorescence spectra of (A) DC-SIGN alone (50 nM), G5-OH (10 nM) + DC-SIGN (50 nM), and G5-OH (10 nM) + DC-SIGN (50 nM) + Mannose; (B) DC-SIGN alone (50 nM), G13- OH (5 nM) + DC-SIGN (50 nM), and G13-OH (5 nM) + DC-SIGN (50 nM) +Mannose; (C) DC-SIGN (30 nM), G27-OH (0.5 nM) + DC-SIGN (30 nM), and G27-OH + DC-SIGN (30 nM) + Mannose; (D) DC-SIGNR alone (50 nM), G5-OH (10 nM) + DC-SIGNR (50 nM), and G5-OH (10 nM) + DC-SIGNR (50 nM) + Mannose; (E) DC-SIGNR alone (50 nM), G13-OH (5 nM) + DC-SIGNR (50 nM), and G13- OH (5 nM) + DC-SIGNR (50 nM) + Mannose; and (F) DC-SIGNR alone (30 nM), G27-OH (0.5 nM) + DC-SIGNR (30 nM), and G27-OH (0.5 nM) + DC-SIGNR (30 nM) + Mannose. Each concentration was done in duplicate and their average fluorescence spectra was used to calculate the QEs.

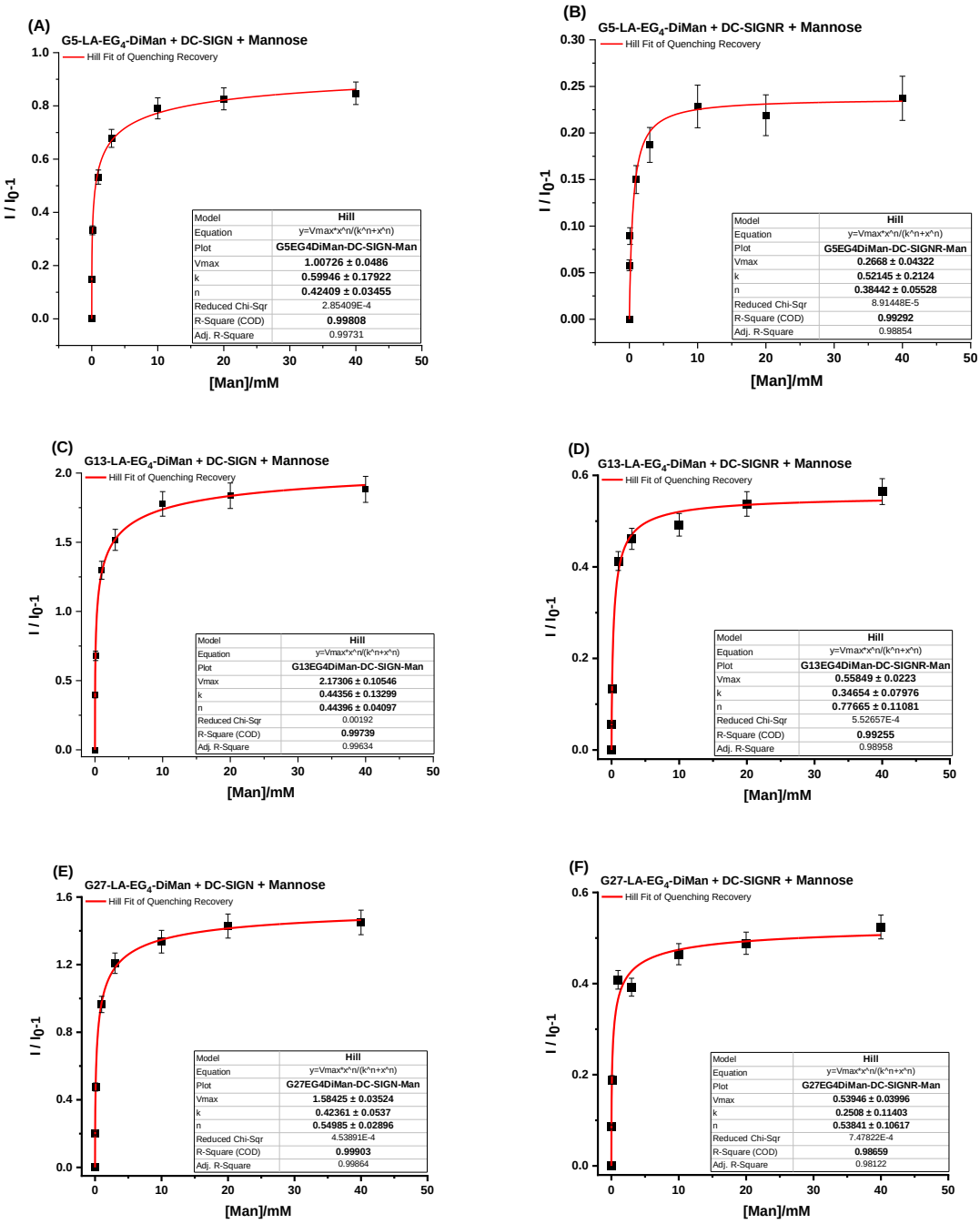

Figure S21. The plots of the fluorescence recovery ratio (I/I_0 - 1) versus concentration free mannose for competing against Gx-DiMan binding with DC-SIGN/R. (A) G5-DiMan + DC-SIGN; (B) G5-DiMan + DC-SIGNR; (C) G13-DiMan + DC-SIGN; (D) G13-DiMan + DC-SIGNR; (E) G27-DiMan + DC-SIGN; and (F) G27-DiMan + DC-SIGNR. The data were fitted by Hill's equation, and the fitting parameters were given in each graph.

Table S3. Summary of the fitting parameters for the fluorescence recovery ratio versus free mannose concentration plots. Where R_{max} (shown as V_{max} in Hill fitting parameters) represents the maximal fluorescence recovery ratio for the Lectin + Gx-DiMan samples with free mannose over that without, and Ki indicates the free mannose concentration giving 50% of maximal fluorescence recovery ratio.

GNP-glycan + Protein	Hill Fitting Parameters			
	R_{max}	Ki (mM)	n	R^2
G5-EG$_4$-DiMan – DC-SIGN	1.01 ± 0.05	0.60 ± 0.18	0.42 ± 0.03	0.998
G5-EG$_4$-DiMan – DC-SIGNR	0.25 ± 0.04	0.52 ± 0.21	0.38 ± 0.05	0.993
G13-EG$_4$-DiMan – DC-SIGN	2.17 ± 0.11	0.44 ± 0.13	0.44 ± 0.04	0.997
G13-EG$_4$-DiMan – DC-SIGNR	0.56 ± 0.02	0.35 ± 0.08	0.78 ± 0.11	0.992
G27-EG$_4$-DiMan – DC-SIGN	1.58 ± 0.04	0.42 ± 0.05	0.55 ± 0.03	0.999
G27-EG$_4$-DiMan – DC-SIGNR	0.54 ± 0.04	0.25 ± 0.11	0.54 ± 0.11	0.986

The maximal fluorescence recovery ratios (V_{max}) observed for DC-SIGN are 3-4 fold higher than those of DC-SIGNR for each GNP-DiMan with different sizes, consistent with that DC-SIGN binding gives stronger fluorescence quenching and hence stronger mannose competition-mediated fluorescence recovery. The K values represent the mannose concentration that give 50% of the maximal fluorescence recovery, which are generally higher for DC-SIGN than for DC-SIGNR. This result is also consistent with the higher binding affinity of DC-SIGN over DC-SIGNR in binding with GNP-DiMan observed in the earlier section.

8. Determination of PGR Ratio for DLS Studies

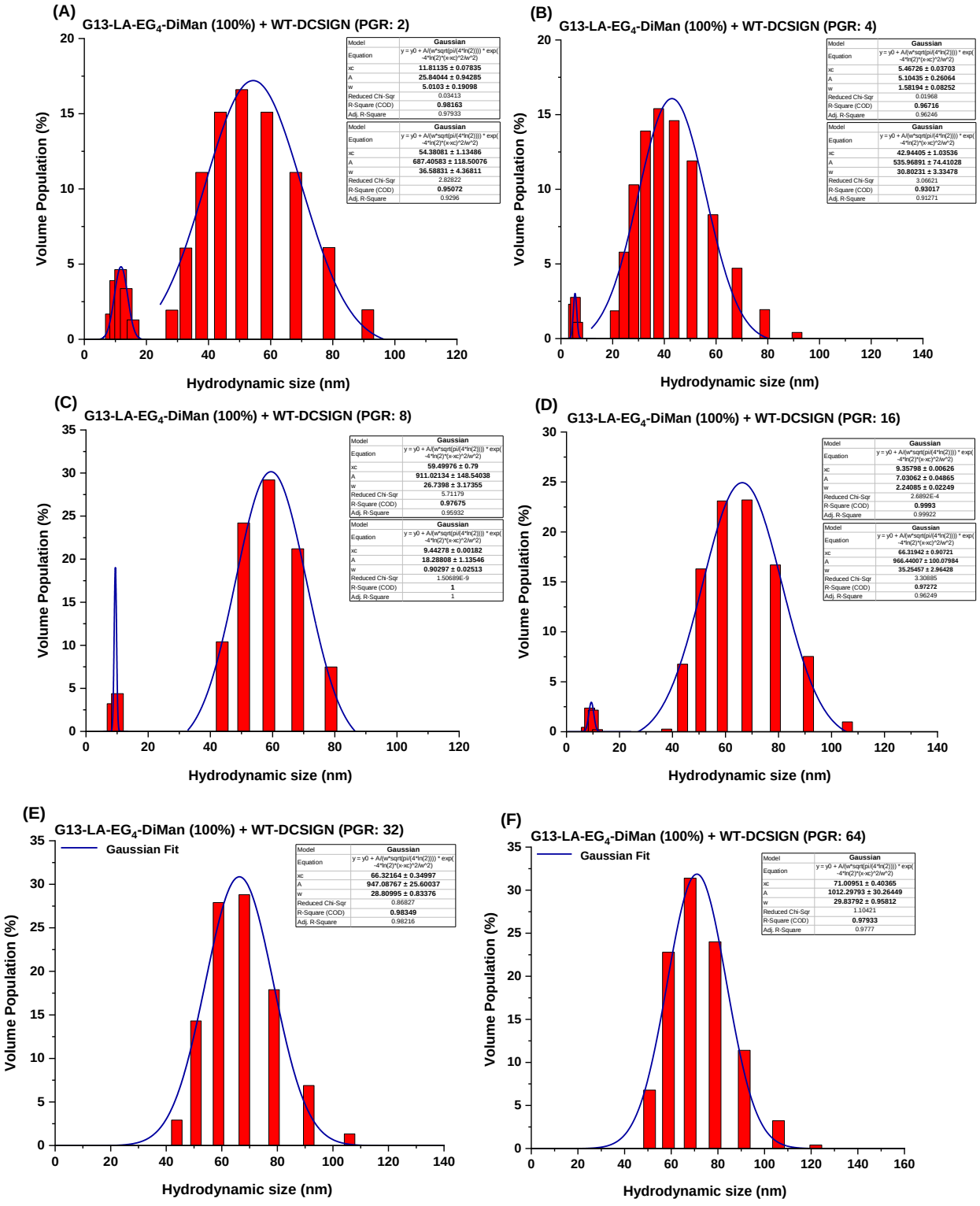

Figure S22. The hydrodynamic diameter (volume population) distribution histograms and Gaussian fits for DC-SIGN binding with G13-DiMan at a PGR of 2 (A); 4 (B); 8 (C); 16 (D); 32 (E); and 64 (F).

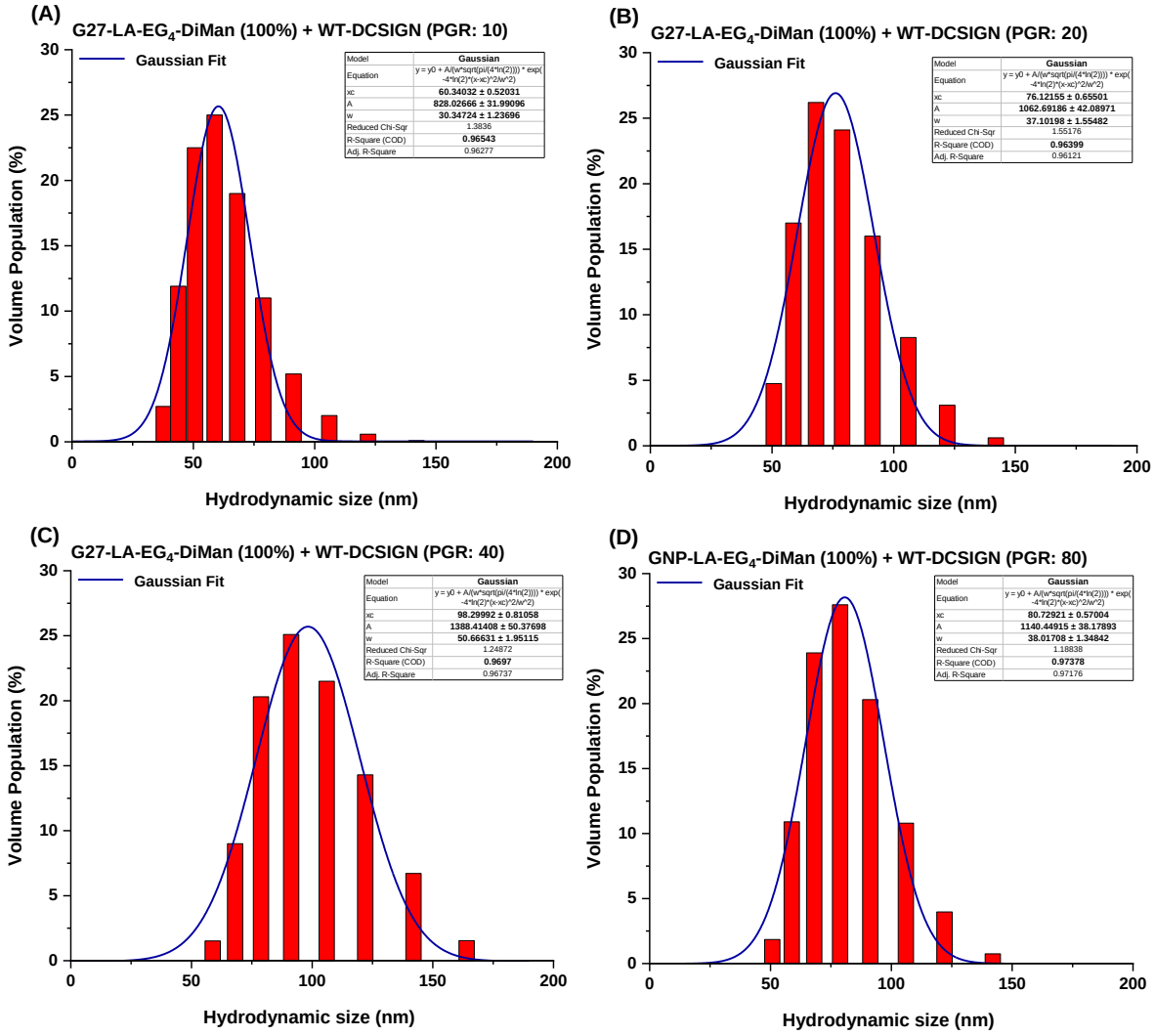

Figure S23. The hydrodynamic diameter (volume population) distribution histograms and Gaussian fits for DC-SIGN binding with G27-DiMan at a PGR of 10 (A); 20 (B); 40 (C); and 80 (D).

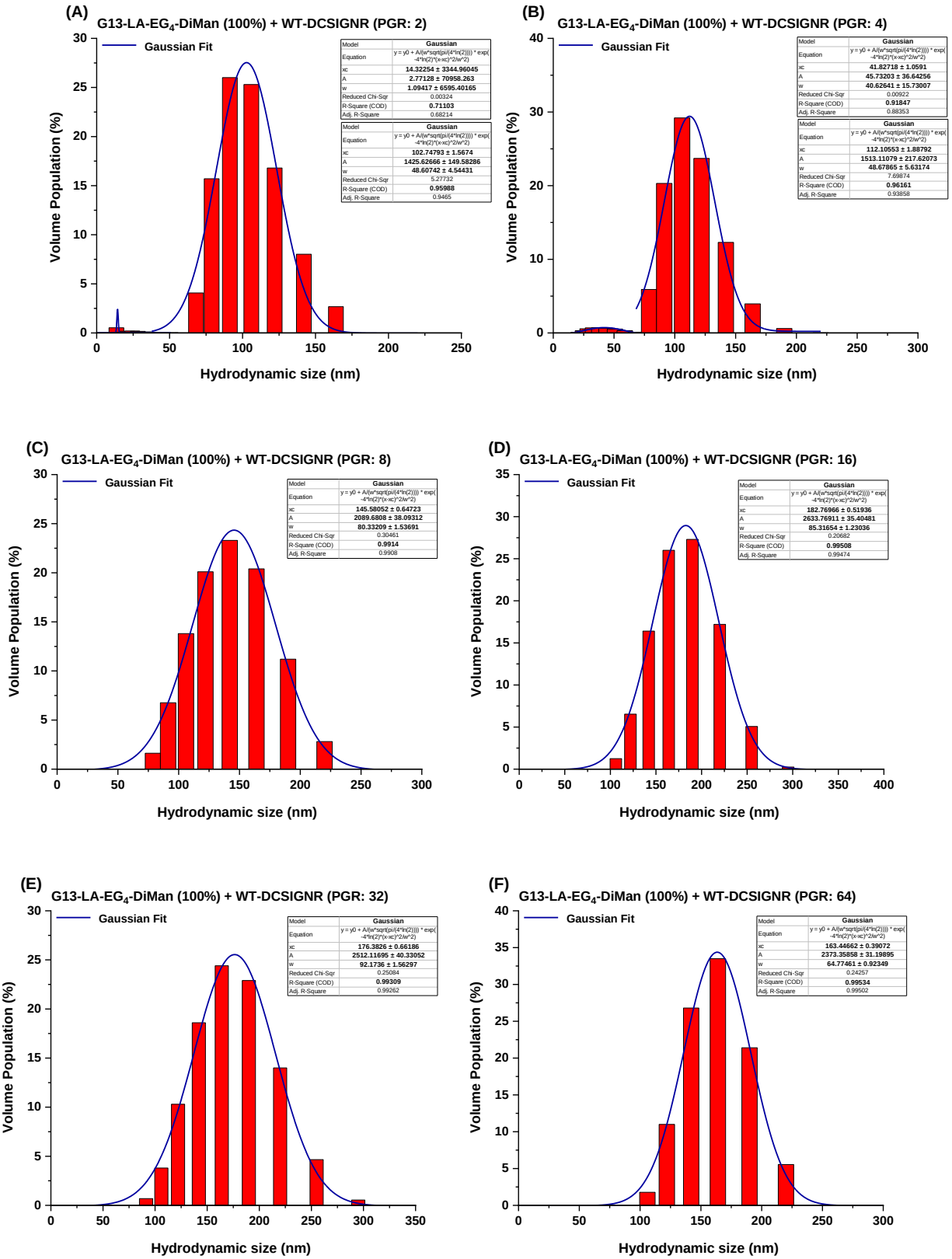

Figure S24. The hydrodynamic diameter (volume population) distribution histograms and Gaussian fits for DC-SIGNR binding with G13-DiMan at a PGR of 2 (A); 4 (B); 8 (C); 16 (D); 32 (E); and 64 (F).

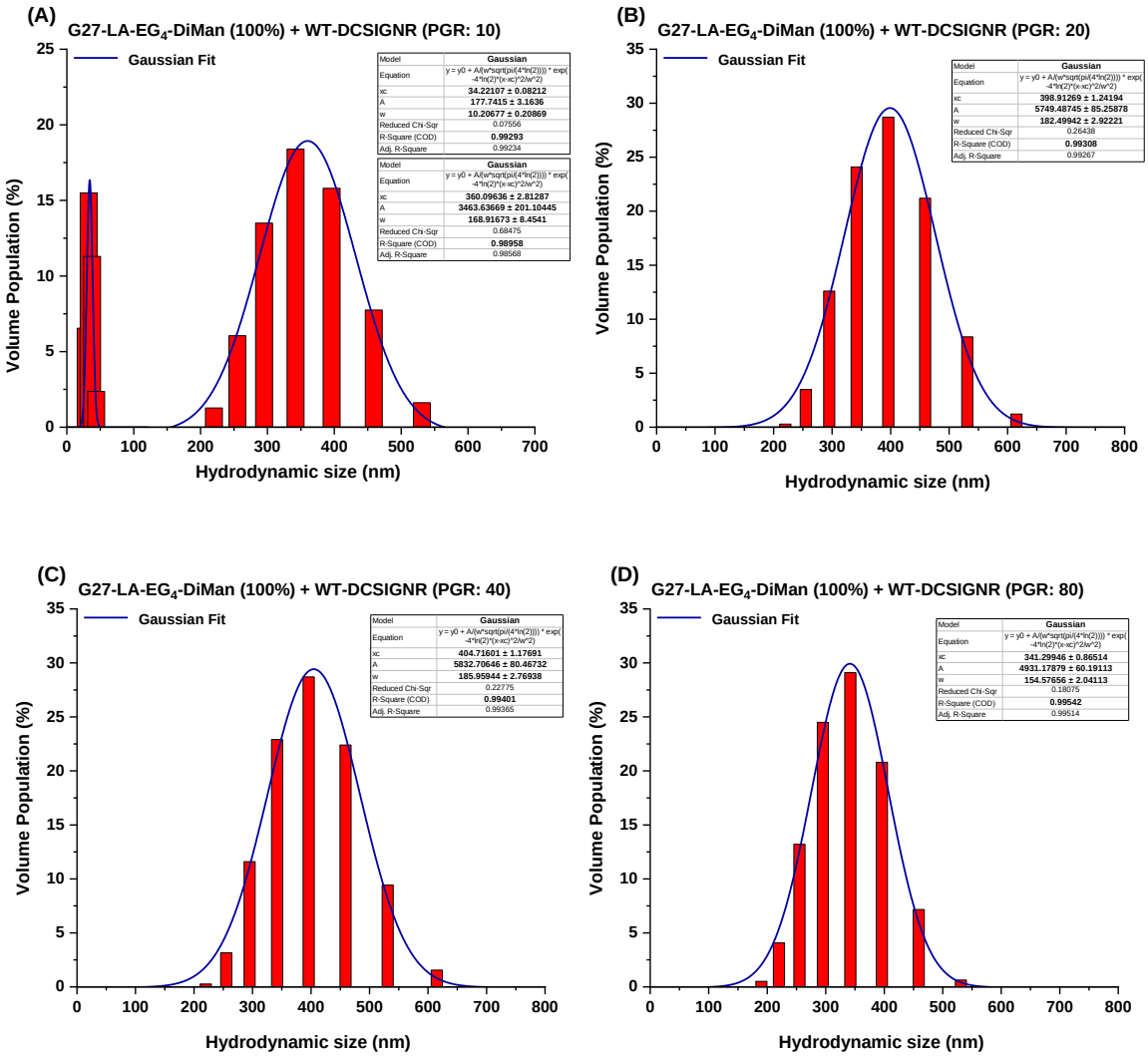

Figure S25. The hydrodynamic diameter (volume population) distribution histograms and Gaussian fits for DC-SIGNR binding with G27-DiMan at a PGR of 10 (A); 20 (B); 40 (C); and 80 (D).

9. Time-dependent D_h Histograms for GNP-glycans binding with DC-SIGN/R

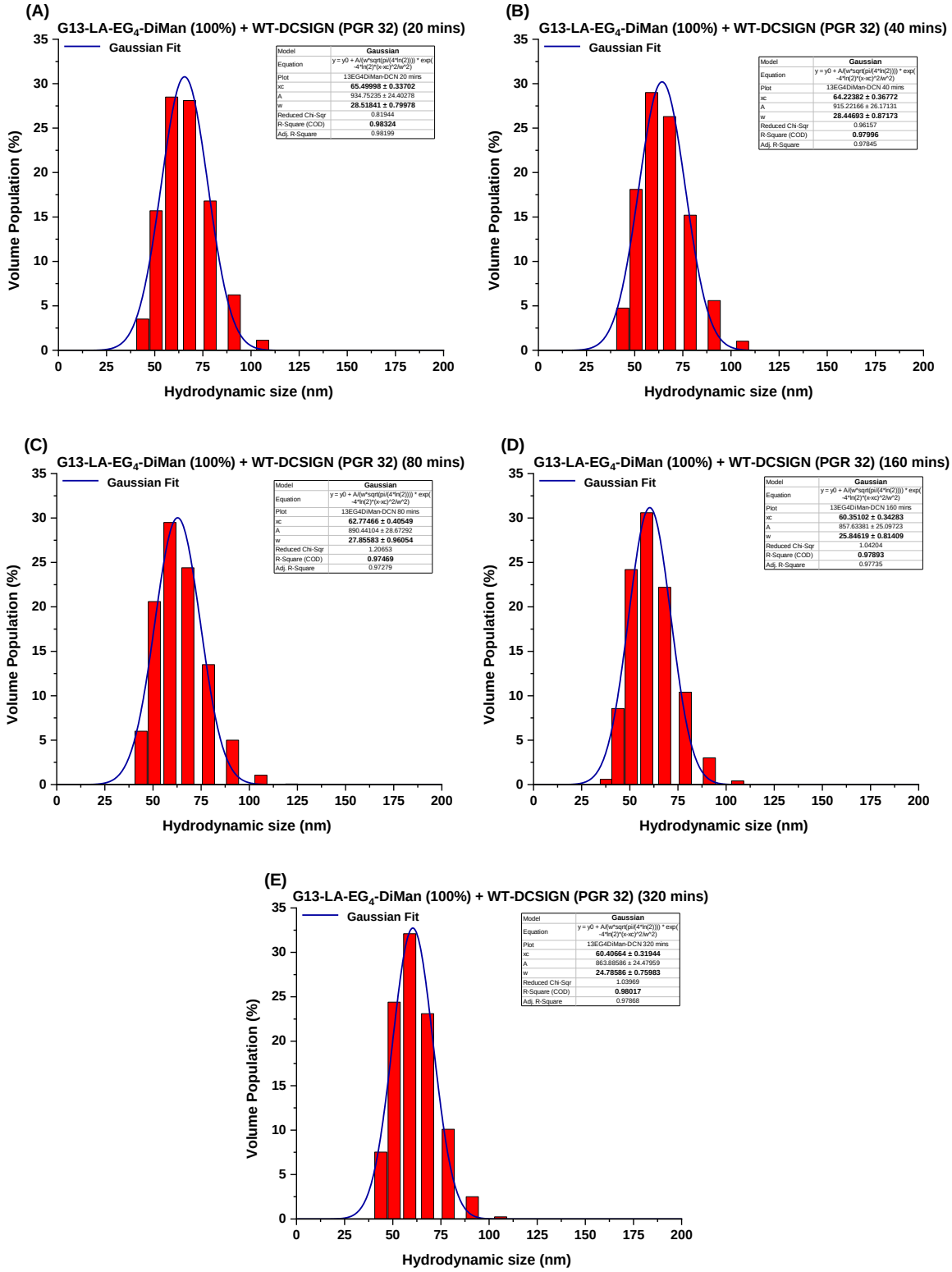

Figure S26. The hydrodynamic diameter (volume population) distribution histograms and Gaussian fits for G13-DiMan binding with DC-SIGN at a PGR of 32 after mixed for 20 (A); 40 (B); 80 (C); 160 (D); and 320 mins (E).

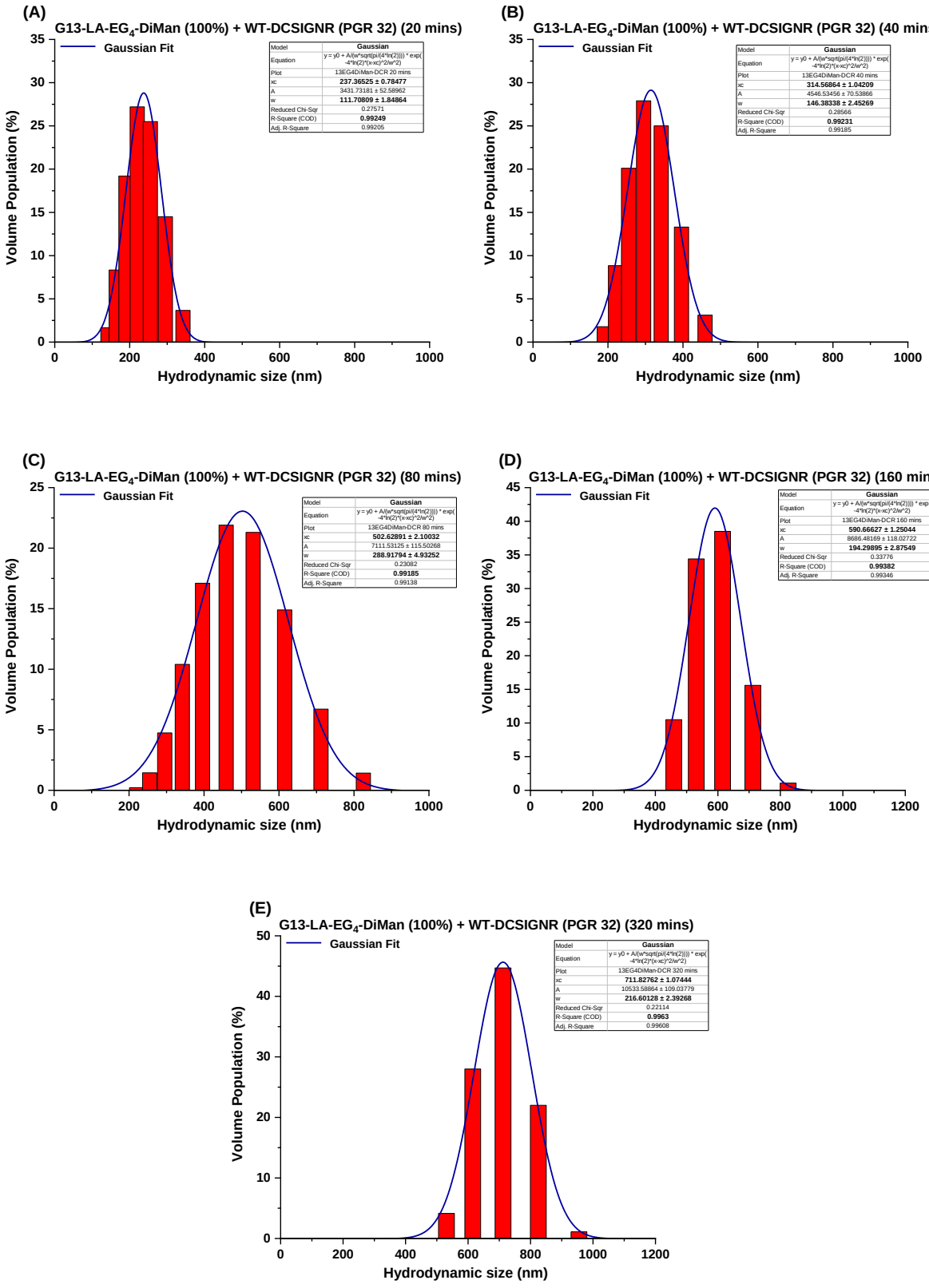

Figure S27. The hydrodynamic diameter (volume population) distribution histograms and Gaussian fits for G13- DiMan binding with DC-SIGNR at a PGR of 32 after mixed for 20 (A); 40 (B); 80 (C); 160 (D); and 320 mins (E).

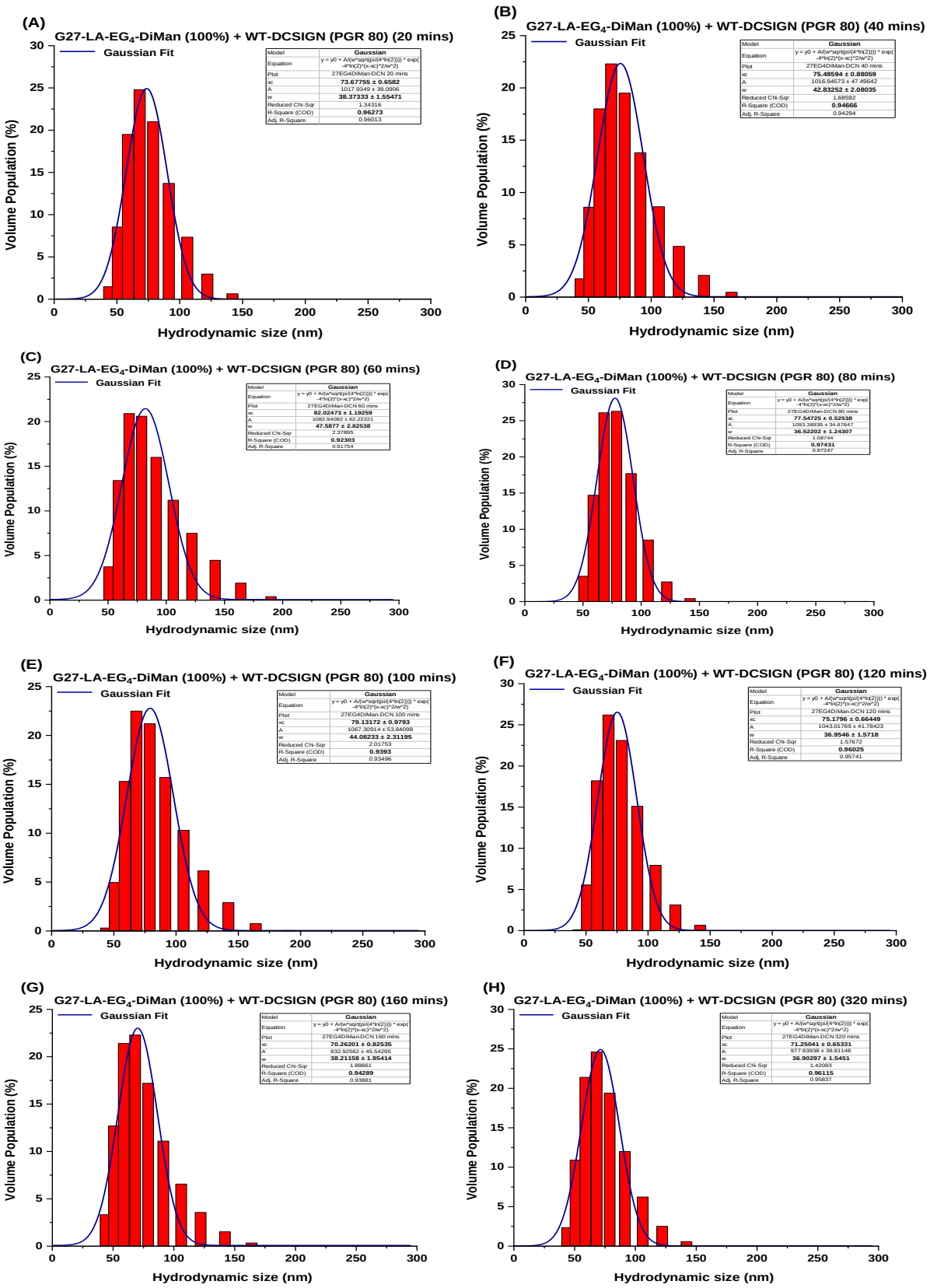

Figure S28. The hydrodynamic diameter (volume population) distribution histograms and Gaussian fits for G27-DiMan binding with DC-SIGN at a PGR of 80 after mixed for 20 (A); 40 (B); 60 (C); 80 (D); 100 (E); 120 (F); 160 (G); and 320 mins (H).

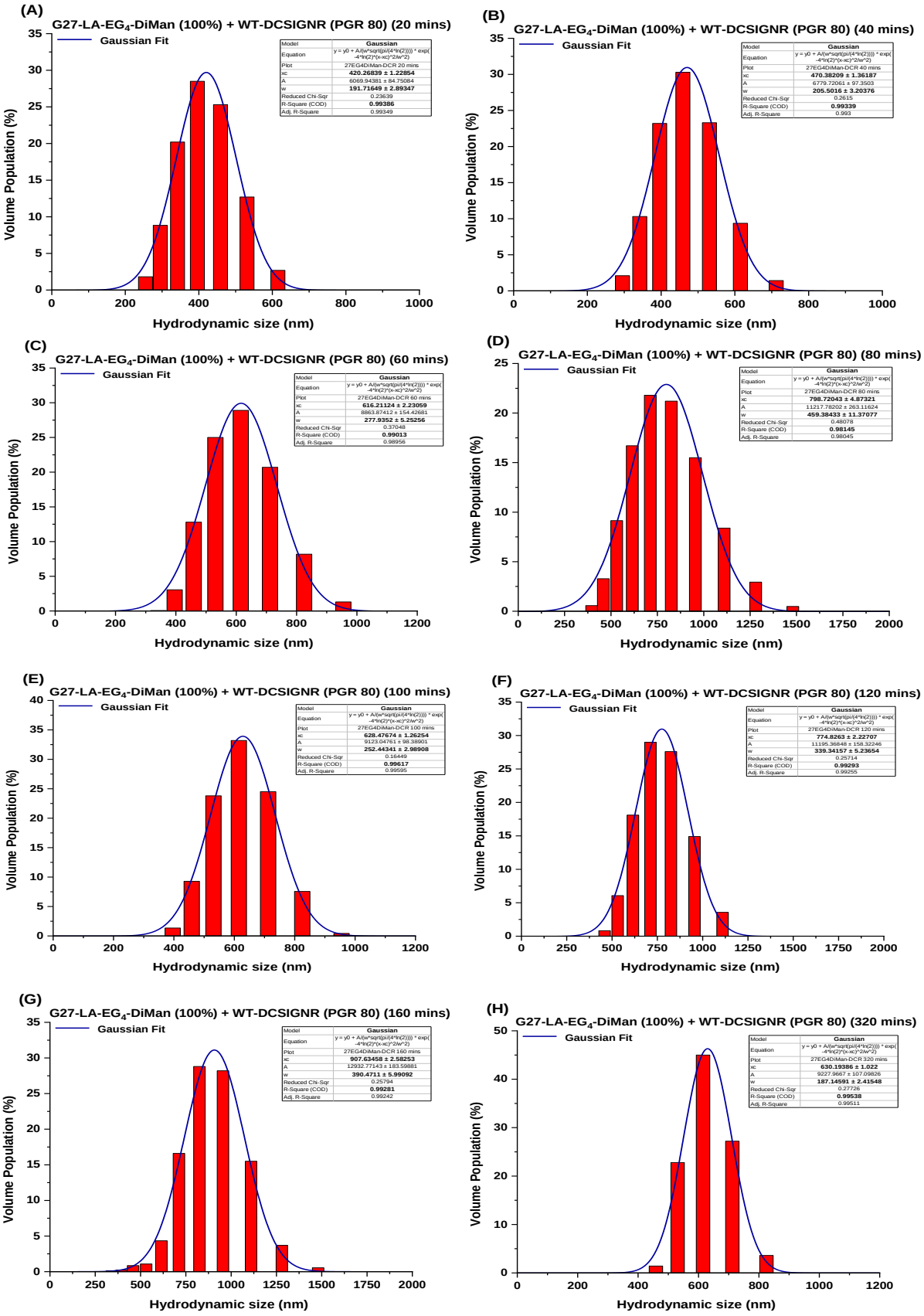

Figure S29. The hydrodynamic diameter (volume population) distribution histograms and Gaussian fits for G27-DiMan binding with DC-SIGNR at a PGR of 80 after mixed for 20 (A); 40 (B); 60 (C); 80 (D); 100 (E); 120 (F); 160 (G); and 320 mins (H).

10. Fluorescence Spectra for DC-SIGN/R Binding Thermodynamics with Gx-glycans.

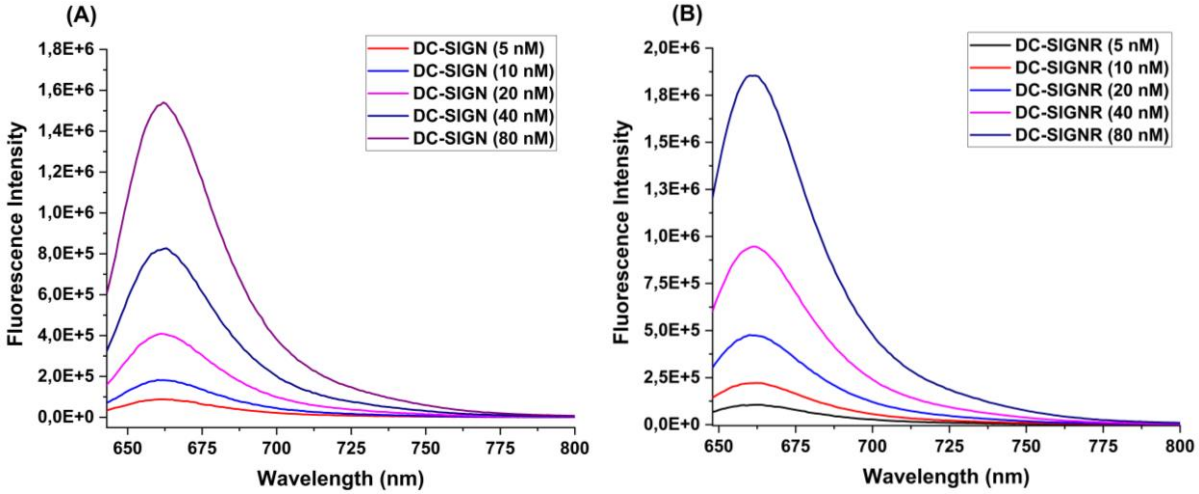

Figure S30. Fluorescence spectra of varying concentrations of Atto-643 labelled (A) DC-SIGN and (B) DC-SIGNR alone in the binding buffer.

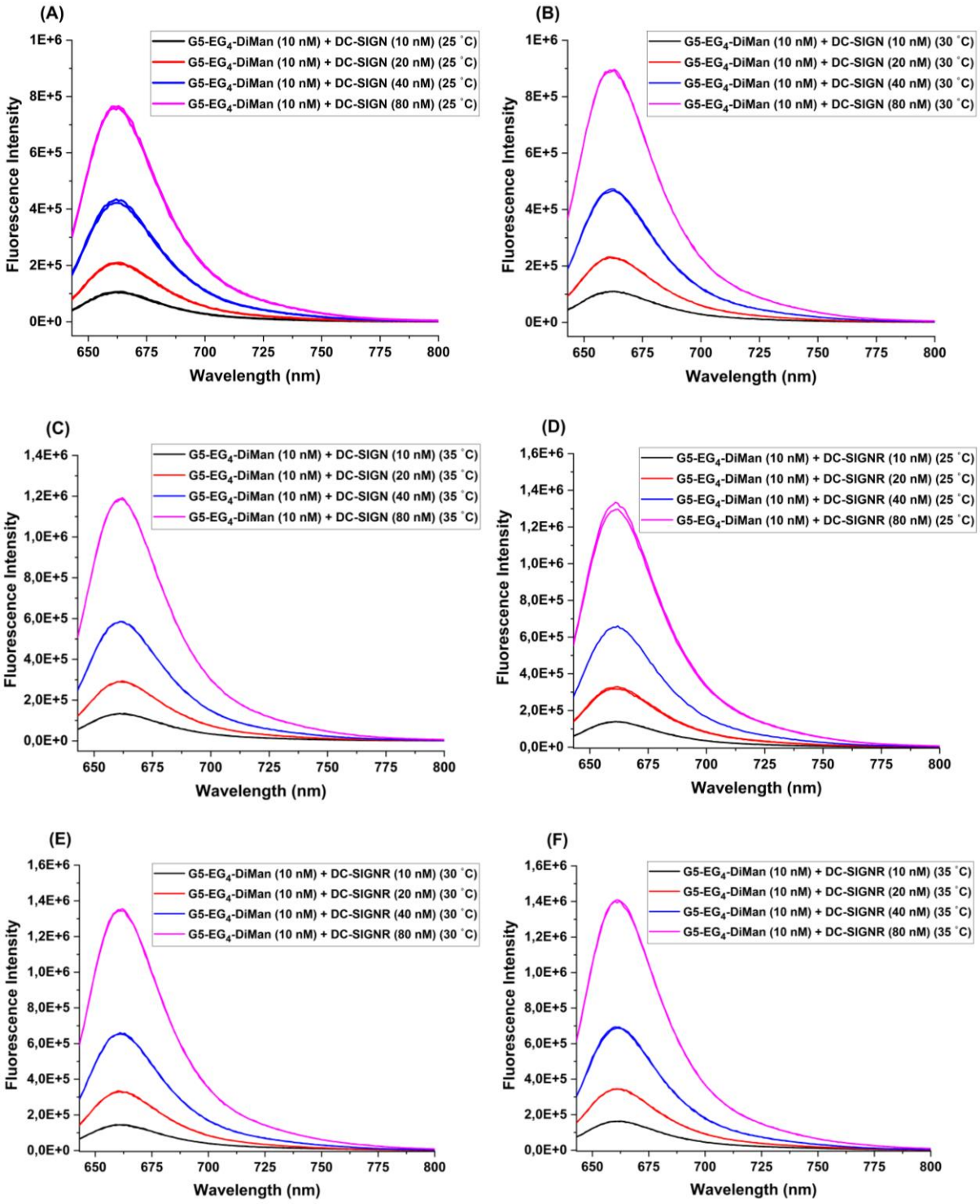

Figure S31. Fluorescence spectra of G5-DiMan (10 nM) after binding to varying concentrations of Atto-643 labelled DC-SIGN at 25 ˚C (A); 30 ˚C (B); and 35 ˚C (C) or Atto-643 labelled DC-SIGNR at 25 ˚C (D); 30 ˚C (E); and 35 ˚C (F). Each concentration was done in duplicate.

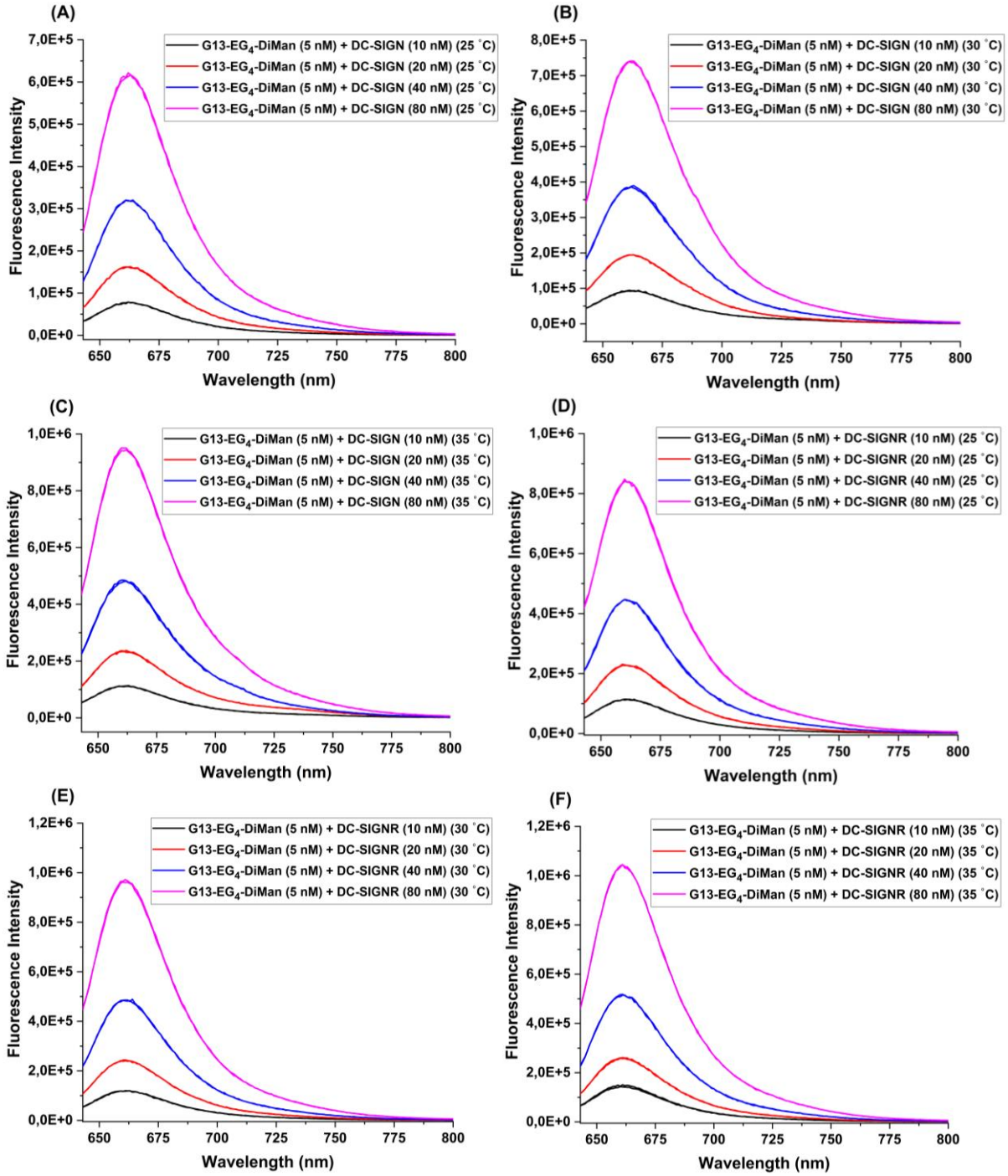

Figure S32. Fluorescence spectra of G13-DiMan (5 nM) + DC-SIGN (varying concentration) at 25 ˚C (A); 30 ˚C (B); and 35 ˚C (C); and G13-DiMan (5 nM) + DC-SIGNR at 25 ˚C (D); 30 ˚C (E); and 35 ˚C (F). Each concentration was done in duplicate, and the average fluorescence was used.

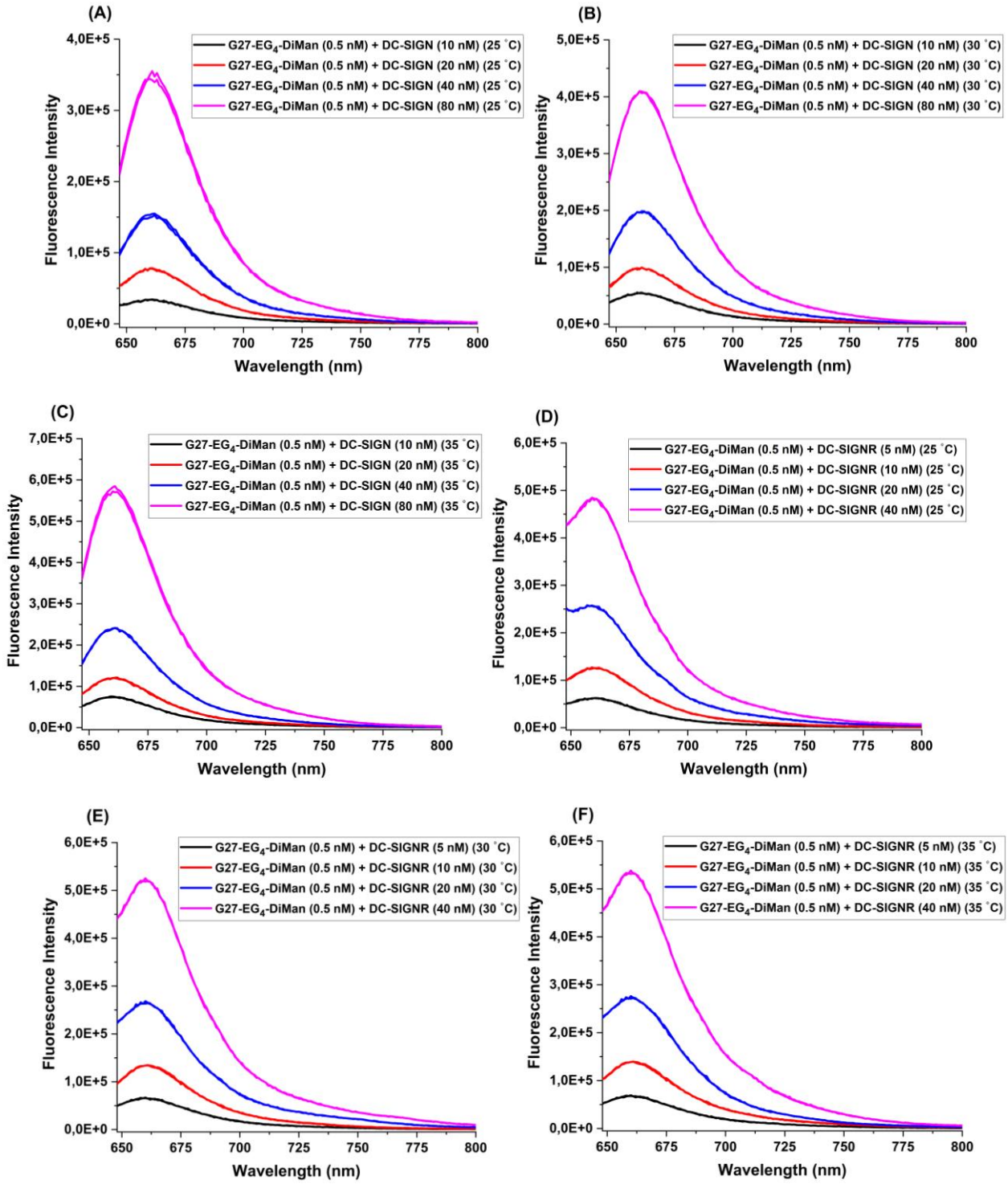

Figure S33. Fluorescence spectra of G27-DiMan (0.5 nM) + DC-SIGN (varying concentration) at 25 ˚C (A); 30 ˚C (B); and 35 ˚C (C); and G27-DiMan (0.5 nM) + DC-SIGNR at 25 ˚C (D); 30 ˚C (E); and 35 ˚C (F). Each concentration was done in duplicate, and the average fluorescence was used.

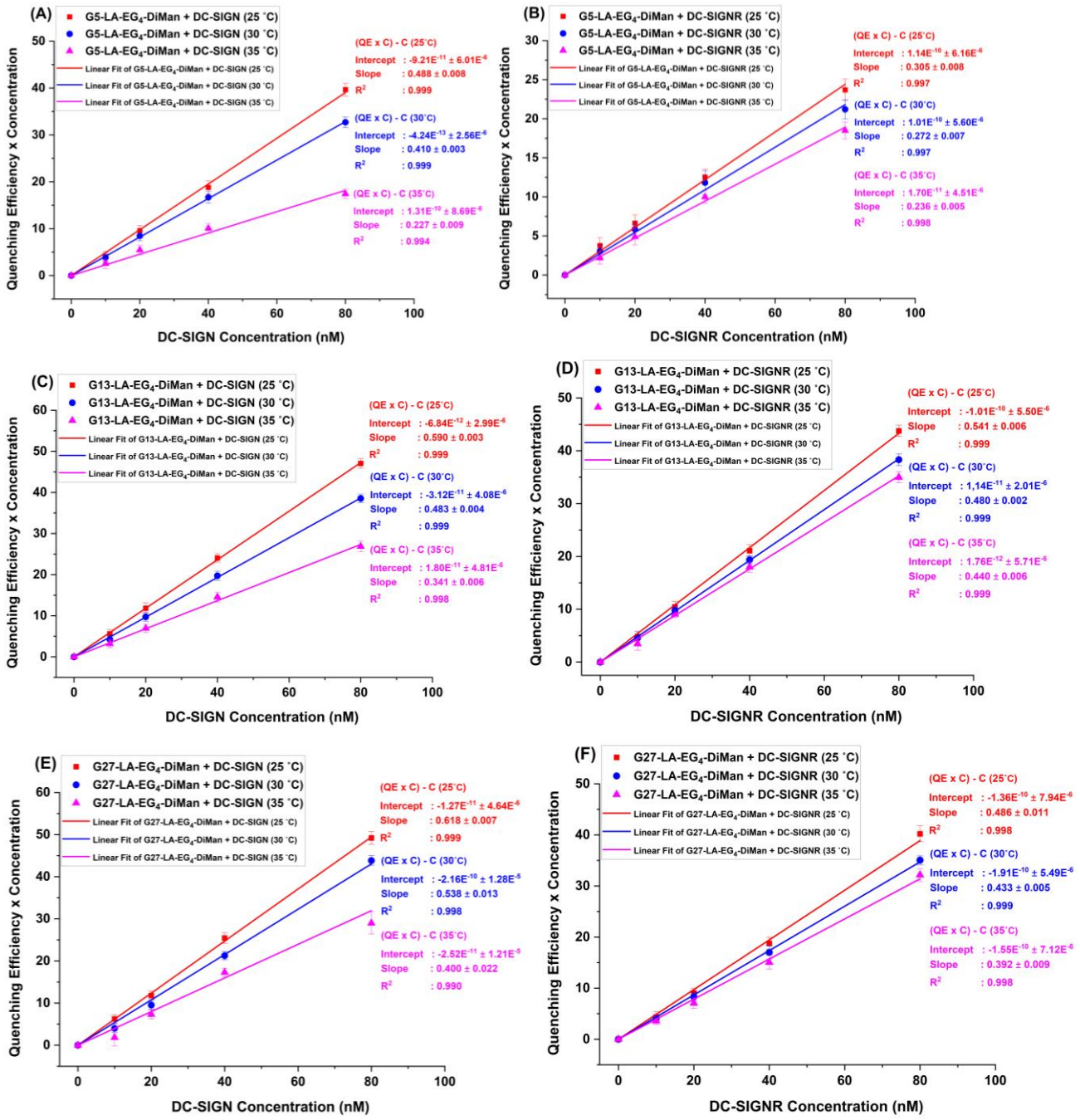

Figure S34. The (QE × *C*) - *C* relationships with linear fits for (A) G5-DiMan+DC-SIGN; (B) G5-DiMan+DC-SIGNR; (C) G13-DiMan+DC-SIGN; (D) G13-DiMan+DC-SIGNR; (E) G27-DiMan+DC-SIGN; (F) G27-DiMan+DC-SIGNR samples at three different temperatures.

Table S4. Summary of the apparent K_d values for Gx-DiMan binding with DC-SIGN/R at varying temperatures. Error bars stand for fitting errors.

GNP-glycans		DC-SIGN		DC-SIGNR	
	T / ºC	**K_d / nM**	**R^2**	**K_d / nM**	**R^2**
G5-DiMan	25	5.4 ± 0.2	0.999	15.8 ± 0.8	0.997
	30	8.5 ± 0.1	0.999	17.6 ± 1.2	0.997
	35	26.3 ± 1.8	0.994	22 ± 1.6	0.998
G13-DiMan	25	1.4 ± 0.03	0.999	2 ± 0.07	0.999
	30	1.8 ± 0.06	0.999	2.8 ± 0.03	0.999
	35	4.1 ± 0.2	0.998	3.5 ± 0.1	0.999
G27-DiMan	25	0.11 ± 0.01	0.999	0.27 ± 0.02	0.998
	30	0.20 ± 0.01	0.998	0.30 ± 0.01	0.999
	35	0.45 ± 0.06	0.990	0.35 ± 0.02	0.998

11. Viral Inhibition Studies

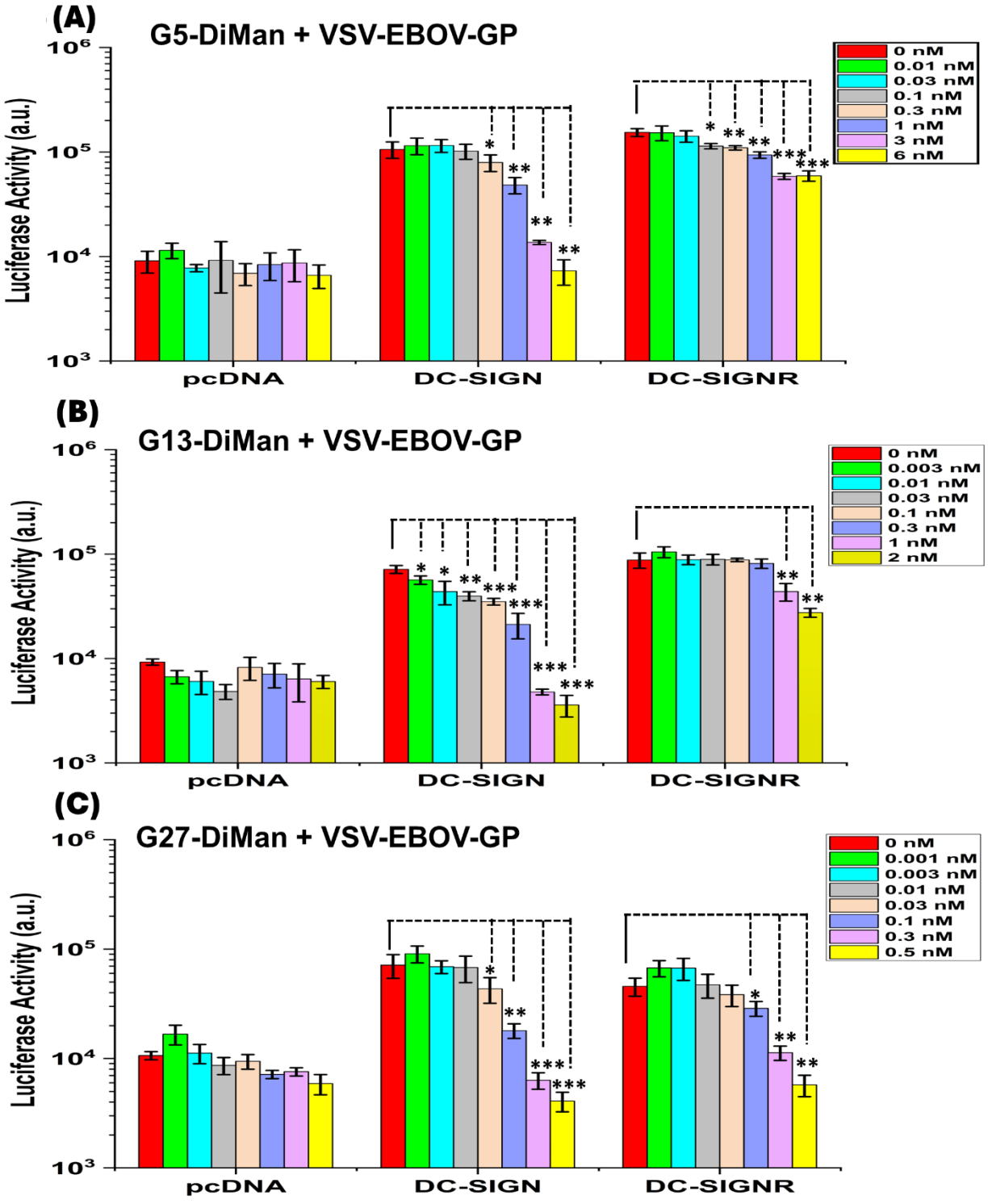

Figure S35. The 293T cellular luciferase activities pre-treated with varying doses of G5-DiMan (**A**), G13-DiMan (**B**) or G27-DiMan (**C**) and then trans-infected with the VSV vector carrying the EBOV-GP. The data are shown as mean ± standard deviations for technical quadruplicates of each sample at each dose from a single experiment. Samples showing no significant statistical differences ($p > 0.05$) from the 0 nM dose controls are not marked while those showing significant statistical differences are marked as *: $p < 0.05$; **: $p < 0.01$; ***: $p < 0.001$.

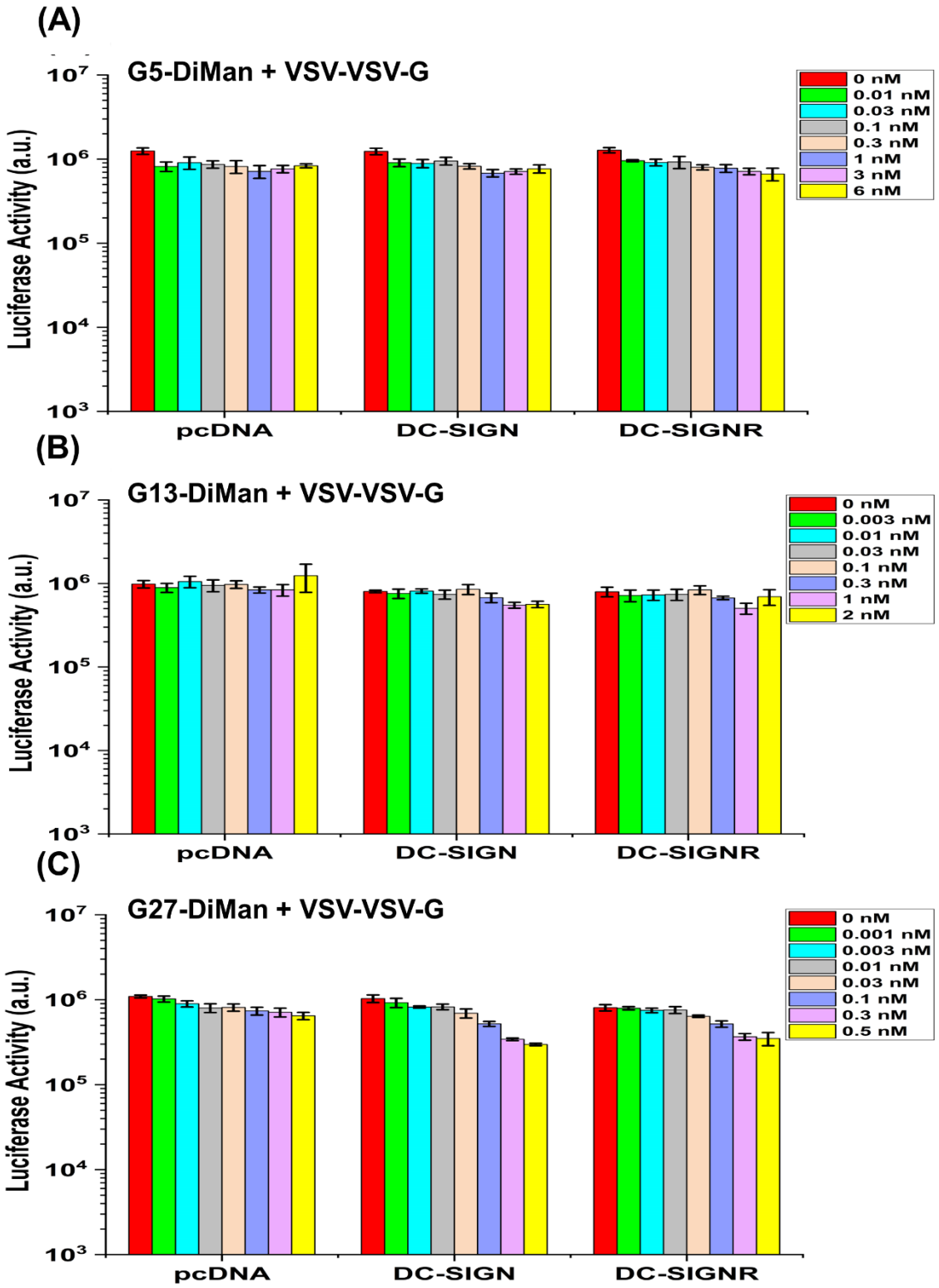

Figure S36. The cellular luciferase activities of 293T cells pre-treated with varied concentrations of G5-DiMan (**A**), G13-DiMan (**B**), or G27-DiMan (**C**) and then trans-infected with the VSV vector particles carrying the control VSV-G proteins. The data are shown as mean ± standard deviations for technical quadruplicates for each sample at each concentration from a single experiment.

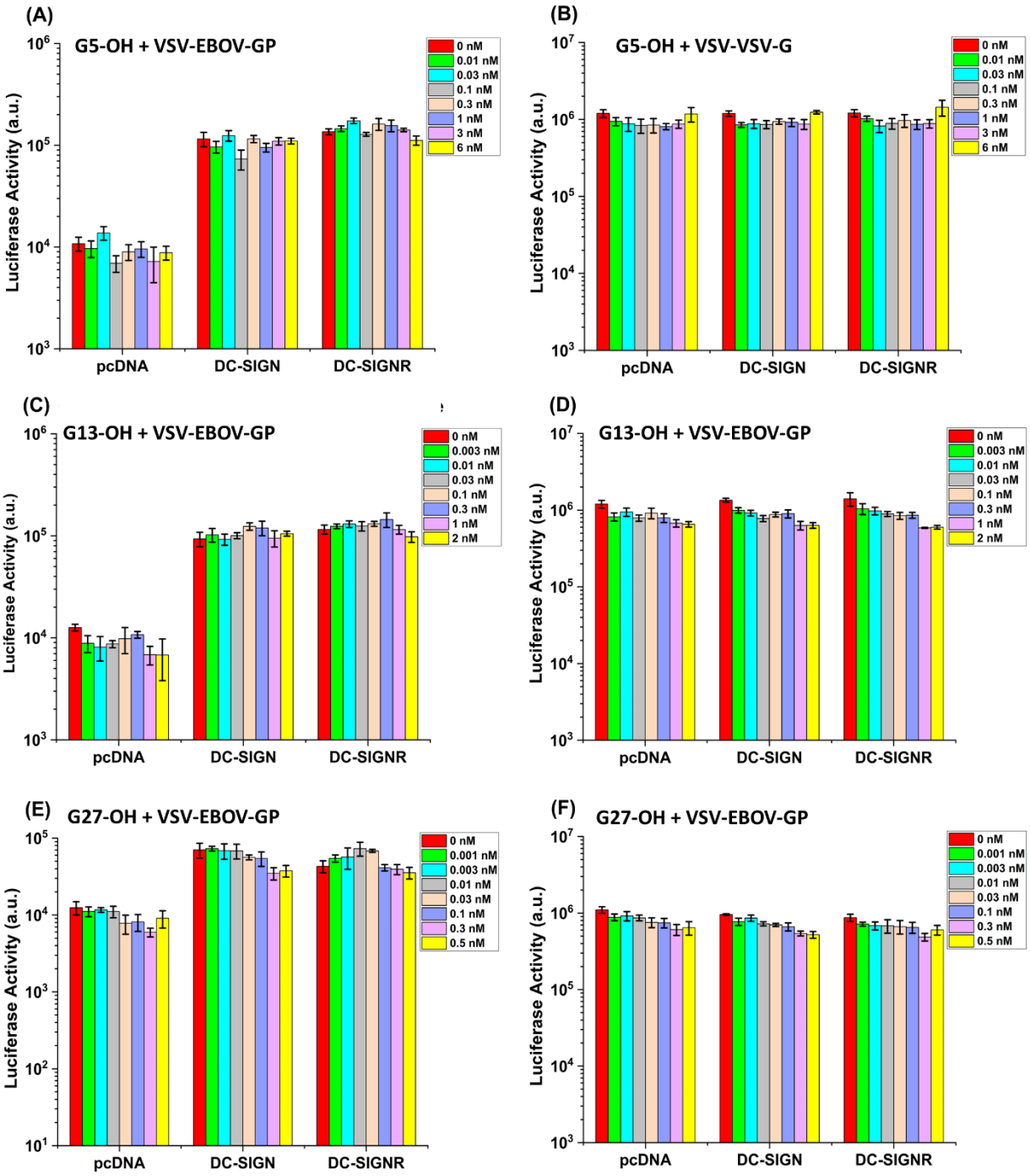

Figure S37. The cellular luciferase activities of 293T cells pre-treated with varied concentrations of G5-OH (**A, B**), G13-OH (**C, D**), and G27-OH (**E, F**) and then trans-infected with the VSV vector carrying the EBOV-GP (**A, C, E**) or the control VSV-G (**B, D, F**). The data are presented here are mean ± standard deviations for technical quadruplicates of each sample at each concentration of a single experiment.

12. Supporting References

1. L. Song, Y. Guo, D. Roebuck, C. Chen, M. Yang, Z. Q. Yang, S. Sreedharan, C. Glover, J. A. Thomas, D. S. Liu, S. R. Guo, R. J. Chen and D. J. Zhout, *ACS Applied Materials & Interfaces*, 2015, **7**, 18707-18716.
2. L. Song, V. H. B. Ho, C. Chen, Z. Q. Yang, D. S. Liu, R. J. Chen and D. J. Zhou, *Adv. Healthc. Mater.*, 2013, **2**, 275-280.
3. X. Ji, X. Song, J. Li, Y. Bai, W. Yang and X. Peng, *J. Am. Chem. Soc.*, 2007, **129**, 13939-13948.
4. D. Budhadev, E. Poole, I. Nehlmeier, Y. Liu, J. Hooper, E. Kalverda, U. S. Akshath, N. Hondow, W. B. Turnbull and S. Pöhlmann, *J. Am. Chem. Soc.*, 2020, **142**, 18022-18034.
5. D. Budhadev, J. Hooper, C. Rocha, I. Nehlmeier, A. M. Kempf, M. Hoffmann, N. Krüger, D. J. Zhou, S. Pöhlmann and Y. Guo, *JACS Au*, 2023, **3**, 1755-1766.
6. Y. Guo, I. Nehlmeier, E. Poole, C. Sakonsinsiri, N. Hondow, A. Brown, Q. Li, S. Li, J. Whitworth, Z. Li, A. Yu, R. Brydson, W. B. Turnbull, S. Pöhlmann and D. Zhou, *J. Am. Chem. Soc.*, 2017, **139**, 11833-11844.
7. Sigma-Aldrich Website - Gold Nanoparticles: Properties and Applications https://www.sigmaaldrich.com/TR/en/technical-documents/technical-article/materials-science-and-engineering/biosensors-and-imaging/gold-nanoparticles.
8. S. K. Saha and C. F. Brewer, *Carbohydr. Res.*, 1994, **254**, 157-167.
9. H. D. Hill, J. E. Millstone, M. J. Banholzer and C. A. Mirkin, *ACS Nano*, 2009, **3**, 418-424.
10. G. B. Stewart-Jones, C. Soto, T. Lemmin, G. Y. Chuang, A. Druz, R. Kong, P. V. Thomas, K. Wagh, T. Zhou, A. J. Behrens, T. Bylund, C. W. Choi, J. R. Davison, I. S. Georgiev, M. G. Joyce, Y. D. Kwon, M. Pancera, J. Taft, Y. Yang, B. Zhang, S. S. Shivatare, V. S. Shivatare, C. C. Lee, C. Y. Wu, C. A. Bewley, D. R. Burton, W. C. Koff, M. Connors, M. Crispin, U. Baxa, B. T. Korber, C. H. Wong, J. R. Mascola and P. D. Kwong, *Cell*, 2016, **165**, 813-826.